Supplement to Sci. Rep. RITU, A, March, 1980

# MELT-QUENCHED AMORPHOUS SUPERCONDUCTING ALLOYS

Akihisa Inoue and Tsuyoshi Masumoto

The Research Institute for Iron, Steel and Other Metals, Tohoku University, Sendai 980.

## ABSTRACT

This paper reviews our current works on melt-quenched amorphous superconducting alloys. Amorphous alloys of Nb-Si, Nb-Mo-Si, Nb-Si-M(M=B, C and Ge), Mo-Si-B, W-Si-B and Ti-Nb-Si system have been found to be superconductors with transition temperatures ranging from 4.2 to 6.8 K. Superconducting properties($T_c$, $H_c$ and $J_c$) are remarkably improved after crystallization upon annealing. The formation of continuous amorphous tapes with highly ductile nature suggests the prospect of alternative methods for the production of superconducting materials.

## 1. INTRODUCTION

Superconducting materials possessing good mechanical properties as well as a high transition temperature($T_c$) are desirable for their applications. Good superconducting materials such as A-15 compounds[1], NaCl-type carbides[2] and C-15 type Laves compounds[3] are extremely brittle at ambient temperature. Such poor mechanical properties prevent these materials from being used under high electrical/magnetic fields and the production of ductile superconductors can alleviate this difficulty. Since it was found [4] that amorphous alloys possess both high strengths and good ductility compared to the crystalline alloys, the expectation that a superconducting material possessing a high $T_c$ as well as good mechanical properties may be obtained in the amorphous state has aroused increasing interest in the study on amorphous superconducting alloys.

The first amorphous superconductor was reported by Buckel and Hilsch[5] in 1954. Amorphous bismuth with a $T_c$ of 6 K was obtained as a thin film by evaporation on a helium-cooled substrate. Since then many investigators have used this method to obtain amorphous metals and alloys[6]. The superconducting metals produced by evaporation on a cold substrate are unstable and generally crystallize below room temperature. In 1975, an amorphous superconducting alloy was obtained by rapid quenching from the liquid state[7]. The samples obtained by melt-quenching can be considered as bulk films in comparison with evaporated films and are very stable at room temperature and above, but they are in the form of circular foils of approximately 1-3 cm diameter and 20-60 μm thickness. Subsequently, in 1978, we have succeeded[8] in producting several refractory metal-based amorphous alloys in the form of a continuous ribbon by using a modified single roller-type quenching apparatus. The continuous ribbon formation of the superconducting materials is very important for practical uses. In the course of further investigations[9-15], we have observed that melt-quenched Nb-, Ti-Nb-based alloys are amorphous and highly ductile. These amorphous alloys have also been found to have a $T_c$ above 4.2 K. This paper reviews our recent results[9-13] on melt-quenched amorphous superconductors, especially the amorphous phase formation ranges of Nb-Si, Nb-M-Si(M=V, Zr, Mo, Ta, W, B, C and Ge), Mo-Si-B, W-Si-B, Ti-Nb-Si and Ti-V-Si systems and the superconducting and mechanical properties of these amorphous alloys.

## 2. ALLOY COMPOSITIONS AND QUENCHING APPARATUS [8-15]

The specimens reported in the present paper are $Nb_{75-85}Si_{15-25}$ binary alloys and $Nb_{80-x}M_xSi_{20}$(M=V, Zr, Mo, Ta and W), $Nb_{80}Si_{20-x}M_x$(M=B, C and Ge), $Mo_{70}Si_{20}B_{10}$, $W_{70}Si_{20}B_{10}$, $Ti_{85-x}Nb_xSi_{15}$, $Ti_{70-x}Nb_{30}Si_x$ and $Ti_{85-x}V_xSi_{15}$ ternary alloys. All compositions are expressed in atomic percent as subscripts. Mixtures of each pure metal(Ti, V, Zr, Nb, Mo, Ta and W), silicon, boron, graphite and germanium were melted in an arc furnace on a water-cooled copper hearth with a tungsten electrode. The melting was accomplished in a purified and gettered argon atmosphere at pressures of about $8 \times 10^4$ Pa. Each alloy was melted 4 or more times to ensure complete mixing of the two or three elements. Weight loss after melting was less than 15 mg in a 30 g ingot, then the composition of alloys reported is expressed by the nominal value.

Continuous ribbons of about 1-2 mm width and 0.02-0.04 mm thickness were prepared from these mother alloys under a protective argon atmosphere using a modified single roller quenching apparatus designed for high melting alloys by the present authors. A schematic illustration of the apparatus is shown in Fig. 1. The alloy is levitation melted at an argon pressure of about 3 MPa, and by opening the shutter and, at the same time, by cutting the coil current off, the molten alloy is ejected by the difference in pressure between the two chambers, through the nozzle at the end of a quartz tube onto the surface of a copper roll which is rotating at a high speed. The ejected melt is solidified on the roll

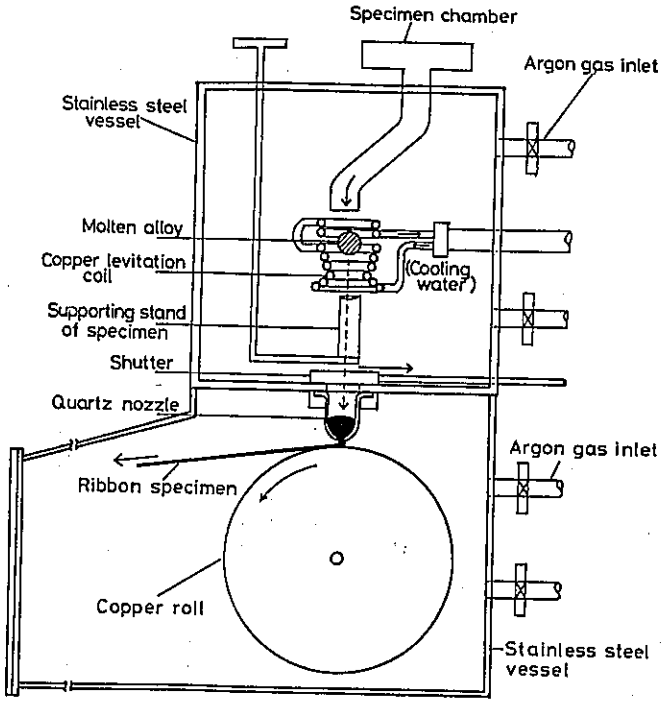


Fig. 1 Schematic illustration of the rapid quenching apparatus used in the present work.

surface in the form of a continuous ribbon. Typically, the amount of alloys melted in one run is about 5 g and the rotation speed of the roll(20 cm in diameter) is about 4000 rpm. This modified melt-quenching apparatus is useful for refractory metals with high melting temperatures and for active metals which easily react with a quartz tube and/or oxygen in air.

## 3. FORMATION RANGE OF AMORPHOUS PHASE [9-12]

Figure 2 shows the composition range in which the amorphous phase formed without any trace of crystallinity for the Nb-Si binary system. Identification of the as-quenched phases was made by conventional method using nickel-filtered Cu K$\alpha$ radiation. The ribbons were classified amorphous when the X-ray intensity as a function of the diffraction angle showed a typical liquid like structure. The amorphous phase forms in a narrow range of 17-21 at% Si around a eutectic point. Also, the amorphous single phase of the Nb-Si alloy is kept by the replacement of silicon with boron up to 12 at%, carbon up to 8 at% and germanium up to 4 at%. Additionally, the formation ranges for $Nb_{80-x}M_xSi_{20}$ (M=V, Zr, Mo, Ta and W), Ti-Nb-Si and Ti-V-Si ternary systems are shown in Figs. 3 to 5. In the figures, the formation of amorphous phase is seen in the alloy composition ranges of 0-20 at% V, 0-25 at% Zr, 0-30 at% Mo, 0-10 at% Ta and 0-10 at% W for Nb-M-Si system, of 0-43

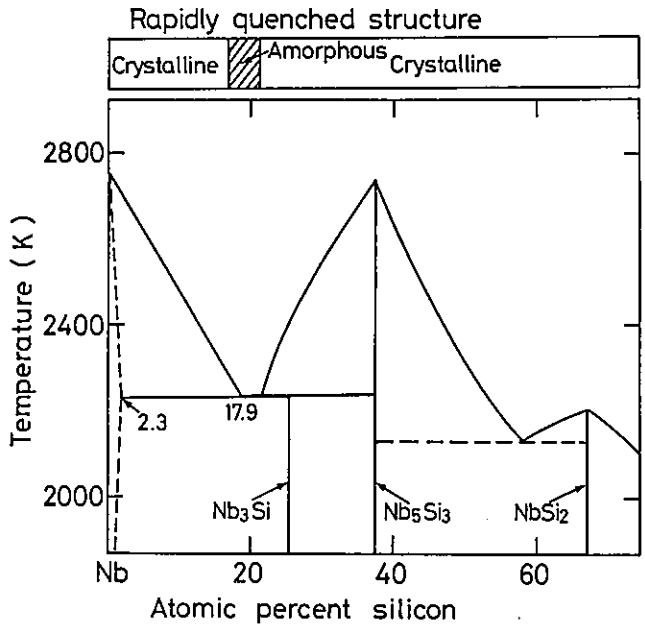


Fig. 2 Composition range for formation of amorphous phase in Nb-Si binary system. Binary phase diagram was obtained from Ref. [17].

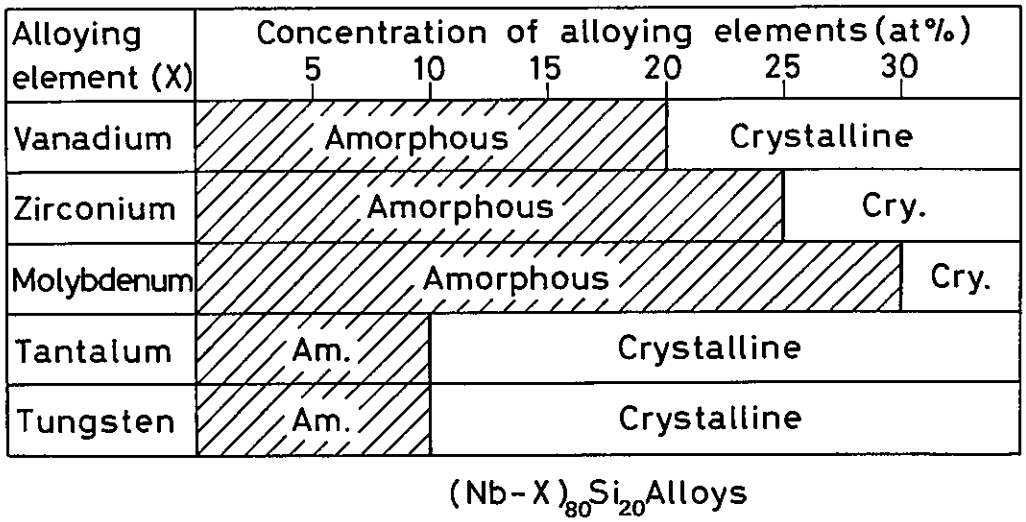


Fig. 3 Composition ranges of amorphous phase formation for the $(Nb\text{-}M)_{80}Si_{20}$ (M=V, Zr, Mo, Ta and W) alloy systems.

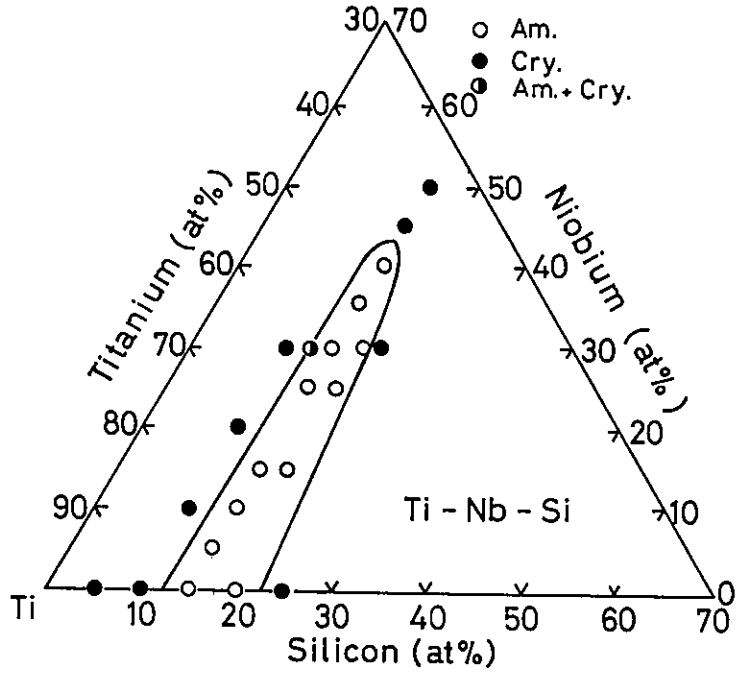


Fig. 4 Composition range for formation of amorphous phase in Ti-Nb-Si ternary system.

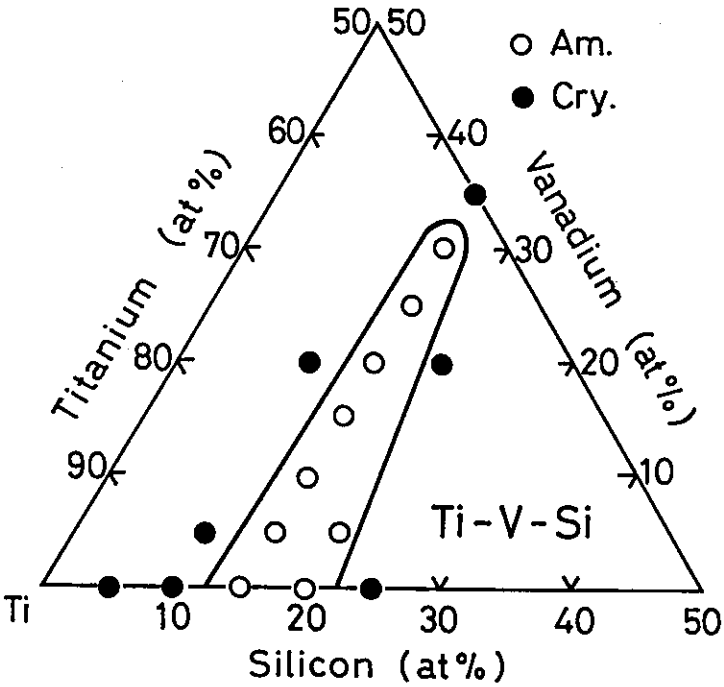


Fig. 5 Composition range for formation of amorphous phase in Ti-V-Si ternary system.

at% Nb and 13-23 at% Si for Ti-Nb-Si system and of 0-32 at% V and 13-23 at% Si for Ti-V-Si system.

In general, the composition range of amorphous alloys obtained by melt-quenching technique is located around a deep eutectic in the alloy phase diagram. Turnbull[16] has noted that a deep eutectic can be interpreted in terms of a comparatively large negative heat of formation of the liquid alloy. Hence, it is predicted that alloys having compositions near a deep eutectic are most prone to the formation of an amorphous phase. Each phase diagram [17] of the Nb-Si, Ti-Si and V-Si binary systems features a eutectic reaction at the composition of $Nb_{82}Si_{18}$, $Ti_{86}Si_{14}$ and $V_{87}Si_{13}$ with a eutectic temperature of 2216 K, 1606 K and 2053 K, respectively. As seen in Figs. 2, 4 and 5, the present amorphous-forming composition ranges also fall near the trough of the eutectics in the Nb-Si binary system and the Ti-Nb-Si and Ti-V-Si ternary systems, as is common in other melt-quenched amorphous alloys, and thus the ability to form an amorphous phase seems to be closely related to the large negative heat of formation of the liquid alloy.

## 4. MECHANICAL PROPERTIES AND CRYSTALLIZATION TEMPERATURE [9-13]

Vickers hardness(Hv), tensile fracture strength($\sigma_f$), crystallization temperature(Tx) and critical fracture temperature($T_f$) of $Nb_{80}Si_{20}$, $Nb_{80-x}M_xSi_{20}$(M=V, Zr, Mo, Ta and W), $Ti_{85-x}Nb_xSi_{15}$ and $Ti_{85-x}V_xSi_{15}$ amorphous alloys are presented in Table 1. Here, Hv and $\sigma_f$ were measured by a Vickers microhardness tester with a 100 g load and an Instron-type tensile testing machine at a strain rate of $1.7 \times 10^{-4}$ /s, respectively. The crystallization temperature of the alloys was examined at a heating rate of $8.33 \times 10^{-2}$ K/s by a differential thermal analyzer(DTA). $T_f$ was defined as the temperature of aging for 6000 s which lead to the fracture of alloys in a simple bend test[18]. The hardness values are in the range of 640-900 DPN for the Nb-based alloys, 550-580 DPN for Ti-Nb-Si alloys and 570-630 DPN for Ti-V-Si alloys and the tensile strengths are in the range 2010-2160 MPa for the Ti-based alloys. Also, the crystallization temperatures are in the ranges of 953-1027 K for the Nb-based alloys, 720-762 K for Ti-Nb-Si alloys and 688-770 K for Ti-V-Si alloys. As seen in the table, there is a tendency that Hv and Tx increase by the replacement of Nb with V, Zr, Mo or W and of Ti with Nb or V. Further, one can notice that the strength and Tx of the Nb-based alloys are superior to those for the Ti-based alloys. This tendency agrees well with that of the bonding forces between Nb-Si and Ti-Si which are presumed from the melting points[19] of $Nb_5Si_3$ and $Ti_5Si_3$ compounds.

Tensile fracture occurs on the shear plane at 45-55 deg to the tensile axis in the direction of thickness, and the fracture surface consists of a smooth part produced by shear slip and a vein-like part produced by plastic instability, similar to the characteristics[20] of general fracture morphology for other transition metal-based amorphous alloys.

Table 1 Vickers hardness(Hv), tensile fracture strength($\sigma_f$), crystallization temperature(Tx) and critical fracture temperature($T_f$) for several refractory metal-based amorphous alloys.

| Alloy system (at%) | Hv(DPN) | $\sigma_f$(MPa) | Tx(K, 5 K/min) | $T_f$(K,×6000s) |
|---|---|---|---|---|
| $Nb_{80}Si_{20}$ | 640 | 2090 | 953 | 780 |
| $Nb_{70}V_{10}Si_{20}$ | 840 | - | 980 | - |
| $Nb_{70}Zr_{10}Si_{20}$ | 715 | 2180 | 987 | 750 |
| $Nb_{70}Mo_{10}Si_{20}$ | 870 | - | 994 | - |
| $Nb_{60}Mo_{20}Si_{20}$ | 895 | - | 1008 | - |
| $Nb_{70}Ta_{10}Si_{20}$ | 805 | - | 966 | - |
| $Nb_{70}W_{10}Si_{20}$ | 895 | - | 1027 | - |
| $Mo_{70}Si_{20}B_{10}$ | 1000 | - | 928 | - |
| $W_{70}Si_{20}B_{10}$ | 1300 | - | 1033 | - |
| $Ti_{70}Nb_{15}Si_{15}$ | 560 | 2060 | 718 | 670 |
| $Ti_{55}Nb_{30}Si_{15}$ | 580 | 2060 | 798 | 670 |
| $Ti_{50}Nb_{35}Si_{15}$ | 625 | 2010 | 870 | - |
| $Ti_{75}V_{10}Si_{15}$ | 570 | 2080 | 738 | - |
| $Ti_{65}V_{20}Si_{15}$ | 610 | 2160 | - | 600 |
| $Ti_{60}V_{25}Si_{15}$ | 645 | 2210 | 762 | 600 |

Furthermore, these amorphous alloys possess a good bend ductility. As an example, deformation structure of $Ti_{55}Nb_{30}Si_{15}$ amorphous alloy bent completely by pressing against the edge of a razor blade is shown in Fig. 6. Numerous deformation markings can be seen

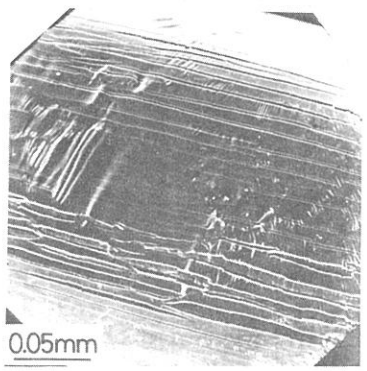


Fig. 6 Scanning electron micrograph showing deformation markings at the tip of $Ti_{55}Nb_{30}Si_{15}$ amorphous alloy bent through 180°.

near the bent edge, and no cracks are observed even after such a severe deformation.

Ductile-brittle transition behavior for $Nb_{80}Si_{20}$, $Nb_{70}Zr_{10}Si_{20}$, $Ti_{70}Nb_{15}Si_{15}$, $Ti_{55}Nb_{30}Si_{15}$ and $Ti_{65}V_{20}Si_{15}$ amorphous alloys was examined as functions of aging time and temperature. As an example, their embrittlement behavior during isochronal aging for 1 h is shown in Fig. 7. The strain on the outer surface required for fracture, $\varepsilon_f$, is estimated from the relation $\varepsilon_f = t/(2r-t)$, where r is the radius of curvature of bent samples at fracture and t is the thickness of ribbon specimens. The temperature for beginning of embrittlement is about 800 K for $Nb_{80}Si_{20}$, 770 K for $Nb_{70}Zr_{10}Si_{20}$ and 600 K for $Ti_{65}V_{20}Si_{15}$ and is lower by about 150-200 K than the crystallization temperatures, while that for $Ti_{55\text{-}70}Nb_{15\text{-}30}Si_{15}$ is about 700 K and is nearly equal to the Tx, indicating that Ti-Nb-Si amorphous alloys remain ductile until the start of crystallization. This result suggests that the decrease in $T_f$ by mixing depends largely on the kind of constituent elements.

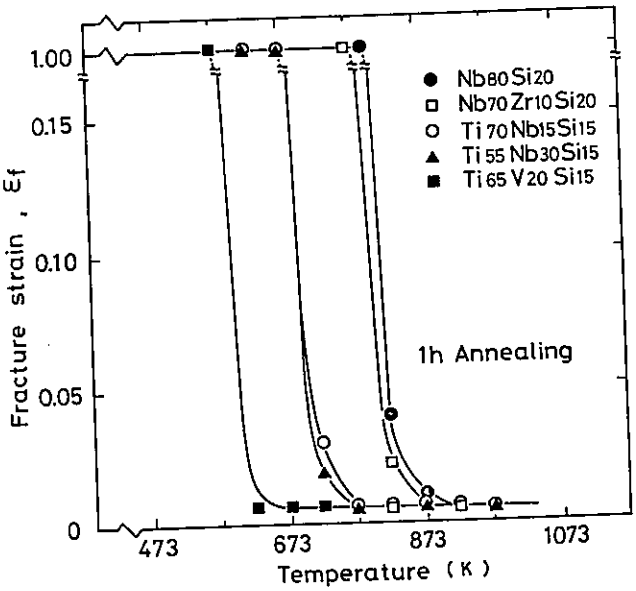


Fig. 7 Change in fracture strain by annealing for 1 h at various temperatures for $Nb_{80}Si_{20}$, $Nb_{70}Zr_{10}Si_{20}$, $Ti_{85\text{-}x}Nb_xSi_{15}$ and $Ti_{65}V_{20}Si_{15}$ amorphous alloys.

## 5. SUPERCONDUCTING PROPERTIES OF THE AMORPHOUS ALLOYS [9-15]

### (1) Transition temperature($T_c$) in the as-quenched state

The superconducting transition was monitored by measuring the resistivity of the material by a conventional four-probe method. The specimen current used is 1 mA. The temperature was

measured using a calibrated Au-Fe + Chromel thermocouple with an accuracy of ±0.05 K. In Fig. 8, the $T_c$ and $\Delta T_c$ of the amorphous alloys for Nb-Si binary system are plotted as a function of silicon content. The value of $T_c$ is taken as the temperature at which R/Rn=0.5, where Rn is the resistance in the normal state. The transition width, $\Delta T_c$, corresponds to the temperature difference between 0.1 and 0.9 of R/Rn. The $T_c$ is 4.4 K for $Nb_{82}Si_{18}$ and has a tendency to decrease slightly with increasing silicon content. If a linear relation is assumed to exist between $T_c$ and silicon content, $T_c$ of $Nb_{75}Si_{25}$ amorphous alloy with $Nb_3Si$ stoichiometric composition is estimated to be about 3.9 K. This extrapolated value agrees well with that($T_c \simeq 3.9$ K)[21] of $Nb_{75}Si_{25}$ amorphous alloy prepared in thin film by covaporation or sputtering. Also, $\Delta T_c$ is of the order of 0.3 K and is much smaller compared with that of the crystalline superconducting alloys indicative of a single phase.

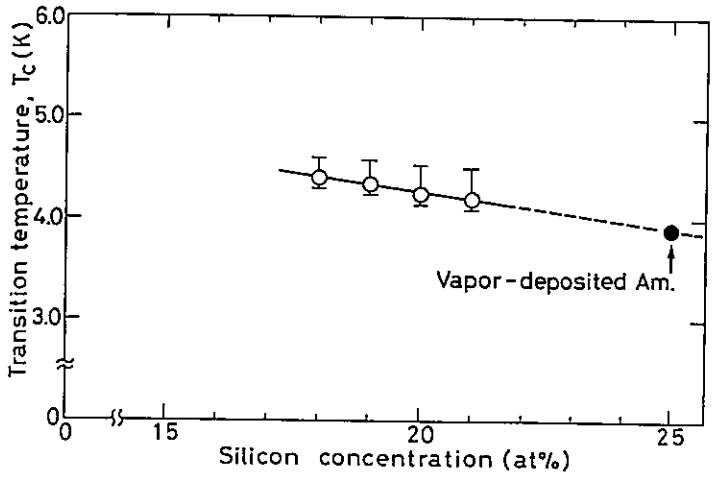


Fig. 8 Silicon concentration dependence of the superconducting transition temperature($T_c$) and the transition width($\Delta T_c$) for Nb-Si amorphous alloys. Vertical bars represent the transition width.

Figures 9 and 10 show the reduced electrical resistance curves measured in no applied magnetic field in the vicinity of $T_c$ for $Nb_{80}Si_{20}$, $(Nb\text{-}M)_{80}Si_{20}$(M=V, Zr, Mo, Ta and W), $Mo_{70}Si_{20}B_{10}$ and $W_{70}Si_{20}B_{10}$ amorphous alloys. The $T_c$ of $(Nb\text{-}Mo)_{80}Si_{20}$ system increases with increasing amount of Mo and attains 5.5 K for the $Nb_{50}Mo_{30}Si_{20}$ amorphous alloy. The addition of V, Zr, Ta or W decreases $T_c$ below the liquid helium temperature(4.2 K), and the onset of the superconducting transition is about 4.1 K for $Nb_{70}V_{10}Si_{20}$ and about 4.2 K for $Nb_{70}W_{10}Si_{20}$, while it can not be detected for $Nb_{60}V_{20}Si_{20}$, $Nb_{70}Zr_{10}Si_{20}$ and $Nb_{70}Ta_{10}Si_{20}$. Thus, the addition of Mo which is at the right hand side of Nb in the periodic table results in an increase in $T_c$. On the other hand, the addition of V, Zr, Ta and W being at the left side of or in dif-

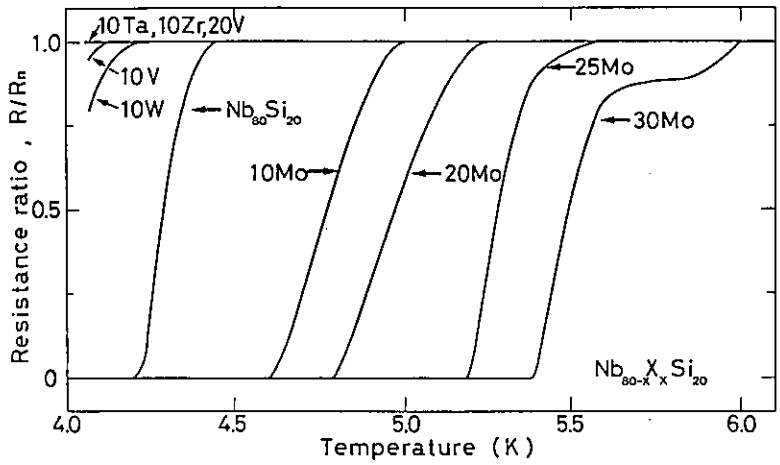


Fig. 9 Resistance ratio R/Rn as a function of temperature for $Nb_{80}Si_{20}$ and $Nb_{80-x}M_xSi_{20}$ (M=V, Zr, Mo, Ta and W) amorphous alloys.

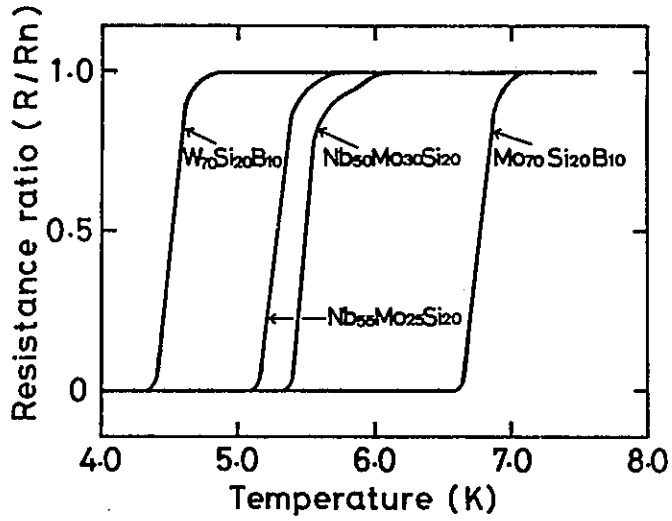


Fig. 10 Resistance ratio R/Rn as a function of temperature for $Mo_{70}Si_{20}B_{10}$ and $W_{70}Si_{20}B_{10}$ amorphous alloys. Also, the data for $Nb_{55}Mo_{25}Si_{20}$ and $Nb_{50}Mo_{30}Si_{20}$ amorphous alloys are shown for comparison.

ferent periods from Nb results in a decrease in $T_c$.

Further, the effect of metalloid elements(B, C and Ge) on the $T_c$ of $Nb_{80}Si_{20}$ amorphous alloy was examined. The replacement of Si by B, C or Ge up to 4 at% resulted in a slight increase in $T_c$. The $T_c$ attained was 4.5 K for $Nb_{80}Si_{16}C_4$ and 4.7 K for both of $Nb_{80}Si_{16}B_4$ and $Nb_{80}Si_{16}Ge_4$.

In addition, one can notice in Fig. 10 that the $T_c$ of $Mo_{70}Si_{20}B_{10}$ and $W_{70}Si_{20}B_{10}$ alloys is 6.8 and 4.5 K respectively. The $T_c$ of Mo-based alloys consisting of 4d transition metal is higher than that for W-based alloys of 5d metal, in conformity with the previous results[22] for the amorphous alloys obtained by vapor-deposition method. Also, the $T_c$ value of $Mo_{70}Si_{20}B_{10}$ is at the same level as those for $(Mo\text{-}Ru)_{80}P_{20}$ amorphous alloys obtained by Johnson et al.[23].

Figures 11 and 12 show the changes of the $T_c$ and $\Delta T_c$ of Ti-Nb-Si amorphous alloys with niobium or silicon content in the case of no applied magnetic field. $T_c$ increases with increasing niobium content or with decreasing silicon content. The highest $T_c$ attained in this ternary system is 5.1 K for $Ti_{45}Nb_{40}Si_{15}$. More recently, it has been found[15] that the replacement of silicon by boron for $Ti_{45}Nb_{40}Si_{15}$ alloy results in an increase of $T_c$ from 5.1 to 5.5 K. In specimens containing less than 10 at% Nb, normal state resistance was observed to remain down to the temperature of liquid helium. The Ti-V-Si amorphous alloys also have $T_c$ down to the temperature of liquid helium even for the specimens containing more than 30 at% V. The $T_c$ value for Ti-Nb-Si-B alloys is much higher than the highest value(4.4 K) reported for ductile binary amorphous Nb-Si alloys and is, within the authors knowledge, the highest among ductile amorphous alloys having completely bent nature. However, the value is about half of those[24,25] reported

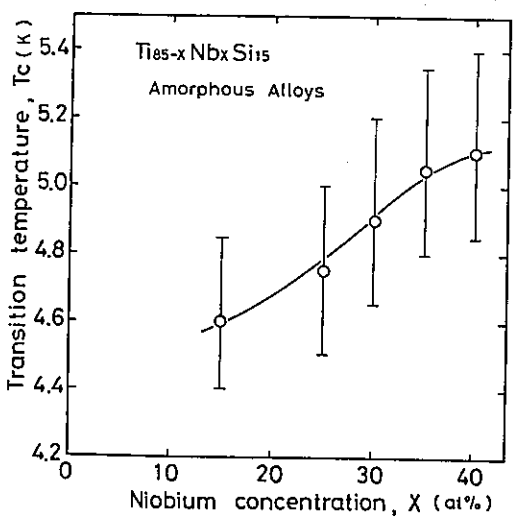


Fig. 11 Niobium concentration dependence of the superconducting transition temperature($T_c$) and the transition width($\Delta T_c$) for $Ti_{85-x}Nb_xSi_{15}$ amorphous alloys. Vertical bars represent the transition width.

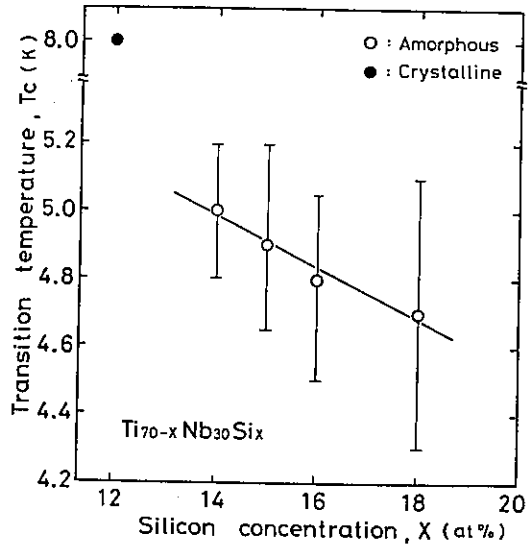


Fig. 12 Silicon concentration dependence of the superconducting transition temperature($T_c$) and the transition width($\Delta T_c$) for $Ti_{70-x}Nb_{30}Si_x$ amorphous alloys. Vertical bars represent the transition width.

for conventional Ti-Nb superconducting materials, indicating that the amorphous state leads to a reduction in $T_c$, similar to many other amorphous superconducting alloys[26] except Mo-based alloys. The effect of additional elements on the $T_c$ of the Ti-Nb based amorphous alloys has not been extensively studied yet and a further enhancement of $T_c$ may be expected by a better design of alloy composition. Also, as seen in Figs. 11 and 12, the transition occurs within a temperature width of about 0.5 K, which is slightly larger compared with the data of the amorphous superconducting alloys[26] reported previously as well as the Nb-Si alloys shown in Fig. 8. Although the reason for such a large transition width in the present alloys is not certain, it may be responsible for the existence of oxygen in the alloys because there is a close correlation[27] between oxygen content and broad transition width.

According to the study on vapor-deposited amorphous metals and alloys by Collver and Hammond[22], the $T_c$ in the amorphous state is related closely to the average outer electron concentration(e/a) showing a broad maximum around [e/a]=6.2-6.4 for the 4d and 5d transition-metal series. This result indicates that the $T_c$ value of the present amorphous alloys increases in the order of Ti, Nb and Mo systems. However, the present result disagrees with the expected order because Ti-based alloys possess higher $T_c$ than Nb-based alloys. In order to examine the reason for such a disagreement, the $T_c$ values of the Nb-Si, $(Nb\text{-}Mo)_{80}Si_{20}$, $Nb_{80}(Si\text{-}M)_{20}$ (M=B, C and Ge), $Mo_{70}Si_{20}B_{10}$ and Ti-Nb-Si amorphous alloys are plotted as a function of the average [e/a] of the transition metal components in Fig. 13 and compared with the variation of $T_c$ for amorphous transition metals obtained by Collver and Hammond.

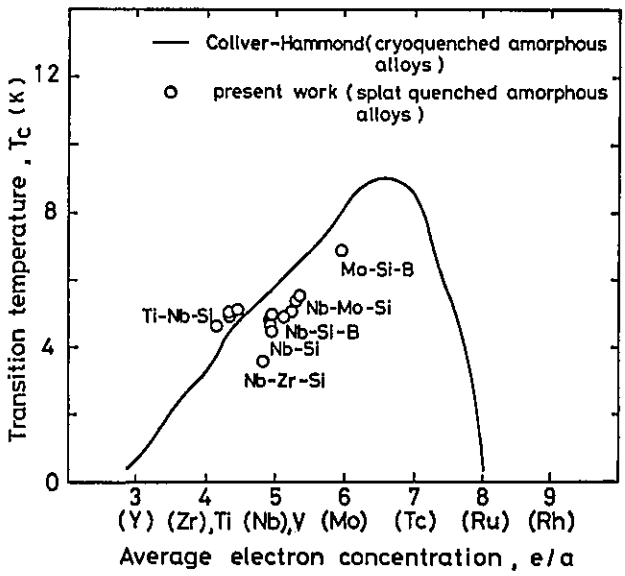


Fig. 13 Superconducting transition temperature($T_c$) versus electron per atom ratio for the 4d transition-metals series. The data for the amorphous vapor-quenched films were taken from Ref. [26].

From this figure, it is seen that the variation of $T_c$ with alloy composition for each alloy system is related apparently to the average e/a. Johnson[23] have shown for $(Mo\text{-}Ru)_{80}P_{20}$ amorphous alloys that such a change of $T_c$ with e/a corresponds well to the change of the electron-phonon bare density of states at the Fermi level($E_f$=0) N(0) with e/a. It has been shown by McMillan[28] that N(0) is one of the most important factors in determining $T_c$. Additionally, one can notice that the $T_c$ values of Nb-Si, Nb-Mo-Si and Mo-Si-B alloys lie below the Collver-Hammond curve. The tendency that $T_c$ values for melt-quenched alloys lie below the Collver-Hammond curve is similar to the results for the other amorphous alloys such as Mo-Ru-P[23], Mo-Ru-B[26], Mo-Re-P-B[26] and Zr-Rh [28,29] systems; namely, when the transition metal components in the alloys are widely separated in e/a and/or the alloys contain metalloid elements, the $T_c$ tends to fall below the Collver-Hammond curve for metals and alloys of neighboring metals. On the other hand, the $T_c$ values of Ti-Nb-Si alloys are higher compared with the Collver-Hammond curve. Although the reason for such an abnormal variation of $T_c$ with e/a is uncertain at present, its origin may be found in one or two of the following two factors: (1) the mixing of the metal elements in different transition metal series, and (2) the oxygen content. Previous reports[26] have shown that the mixing between metal elements in different series results in the decrease of $T_c$ of amorphous alloys. On the other hand, it has been reported[27] that the addition of a small amount of oxygen apparently raises $T_c$ of crystalline Ti-Ta alloys significantly. This fact suggests that the $T_c$ higher than the value expected from Collver-Hammond curve may be due to a small amount of oxygen contained in the Ti-Nb-Si amorphous alloys. The occurrence of such a high $T_c$ has been also recognized[15] for Ti-Nb-Si-B amorphous alloys. It is hoped that more systematic investigations on the effect of a small amount of impure elements such as oxygen or nitrogen on $T_c$ will be made in near future.

(2) Effect of cold-working on the transition temperature($T_c$)

Investigation on the effect of cold-working on $T_c$ of amorphous alloys is very important for practical uses, because of the possibility that the alloy would be deformed to a final shape. The $T_c$ values of cold-rolled $Ti_{70}Nb_{15}Si_{15}$ and $Ti_{55}Nb_{30}Si_{15}$ amorphous alloys are plotted as a function of the reduction in area in Fig. 14. The $T_c$ value is a little change until 15% reduction, but with further increasing reduction it lowers rapidly and fall to about 4.2 K after about 40% reduction. However, it can be noticed in Fig. 14(b) that the $T_c$ recovers to the nearly previous level by annealing for 1 h at 573 K which is much lower than the crystallization temperatures. In addition, there was no change in good ductile nature of these alloys. Consequently, the lowering of $T_c$ by cold-rolling seems not to be a serious problem for practical uses of amorphous superconductors. We believe that such a lowering of $T_c$ is due to the internal strain introduced in amorphous structure by cold-working.

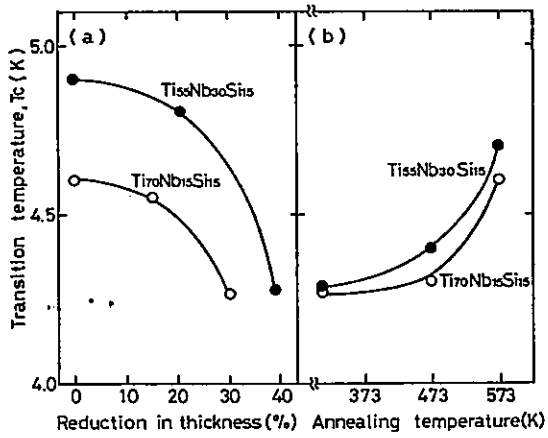


Fig. 14 (a) Change in superconducting transition temperature($T_c$) of $Ti_{70}Nb_{15}Si_{15}$ and $Ti_{55}Nb_{30}Si_{15}$ amorphous alloys by cold rolling.
(b) Change in superconducting transition temperature($T_c$) of cold-rolled $Ti_{70}Nb_{15}Si_{15}$ and $Ti_{55}Nb_{30}Si_{15}$ amorphous alloys by annealing.

(3) Effect of low-temperature annealing on the transition temperature($T_c$)

It has been pointed out[30-32] that Fe- and Co-based amorphous alloys obtained by melt-quenching exhibit improved magnetic properties when annealed at temperatures sufficiently low as to produce no crystallization. Stress relaxation[32], embrittlement [16,32] and a change in the atomic pair correlation function[33] have also been observed as a result of such low-temperature annealing. Considering such an effect by low-temperature annealing we expected a similar effect on the superconducting properties which are strongly affected by the microscopic structure of the material.

A change in the $T_c$ of $Ti_{55}Nb_{30}Si_{15}$ amorphous alloy with annealing temperatures is shown in Fig. 15, wherein the structure and the ductility after annealing are also represented for comparson. "Ductile" implies that complete bending through 180° is possible without breaking and "brittle" implies that the alloy fractures during bending. The $T_c$ remains practically unchanged up to about 500 K. However, the value begins to decrease around about 550 K and shows a minimum(about 4.1 K) at about 670 K followed by a rapid increase. As seen in the figure, the remarkable increase in the $T_c$ at higher temperatures above about 700 K is due to the precipitation of a crystalline phase(Ti(Nb) solid solution with bcc structure)[10]. Figure 16 shows bright field images and selected area diffraction patterns of the as-quenched (a and b) and annealed(c and d) $Ti_{55}Nb_{30}Si_{15}$ amorphous alloys. As seen in the diffraction pattern(d), the amorphous structure remains unchanged

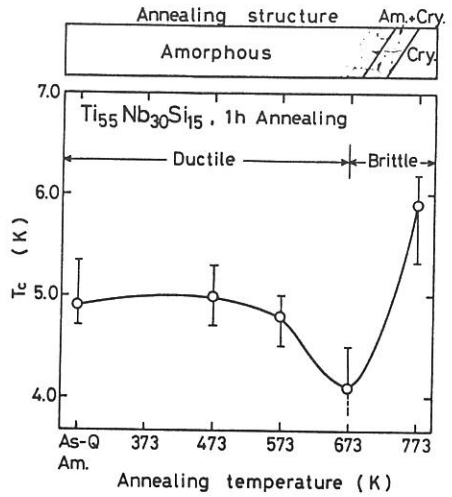


Fig. 15 Change in superconducting transition temperature($T_c$) of $Ti_{55}Nb_{30}Si_{15}$ amorphous alloy upon annealing for 1 h at various temperatures.

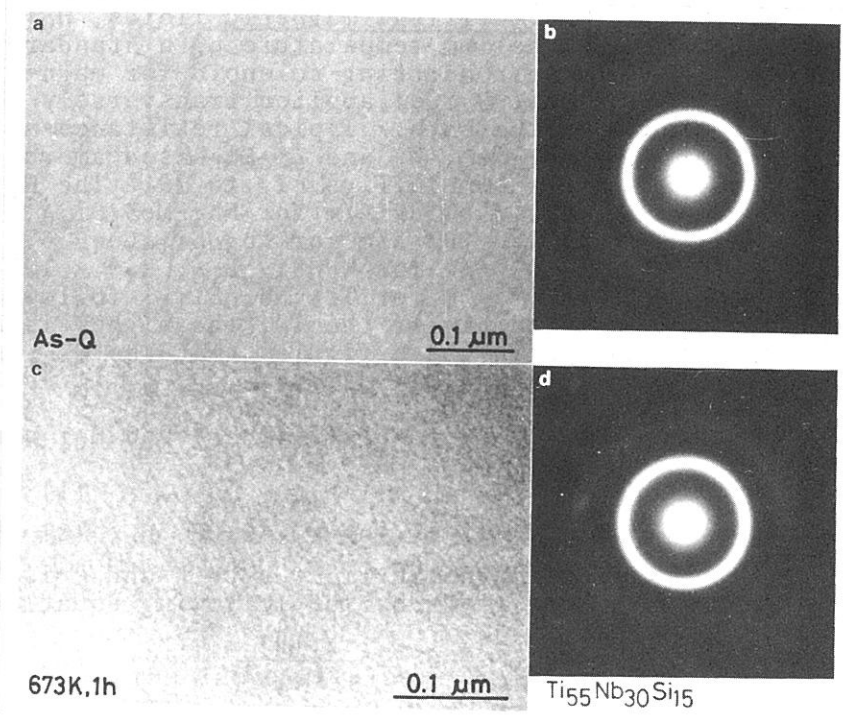


Fig. 16 Transmission electron micrographs and selected area diffraction patterns showing the as-quenched structure(a and b) and the structure after annealing for 1 h at 673 K (c and d) of $Ti_{55}Nb_{30}Si_{15}$ amorphous alloy.

even after annealing for 1 h at 673 K. But in the highly magnified bright field image(c), a fine weak contrast can be seen innumerably all over the photograph, indicating a microscopic change in the amorphous structure. Hence, it is suggested that the decrease in the $T_c$ upon low-temperature annealing is due to the structure relaxation or short-range ordering of the amorphous structure. Thus, an improvement of superconducting properties can not be achieved by annealing treatments below the crystallization temperature. The decrease in $T_c$ upon low-temperature annealing has also been recognized for amorphous Zr-Rh[34] and Nb-Si[9] binary alloys.

In general, it has been known that the $T_c$ is a function of several microscopic parameters which characterize the d-band structure. However, an explanation of the low-temperature annealing effect on $T_c$ seems to be very difficult because one would need further knowledges of the microscopic atomic configurations and their theoretical connection with the microscopic parameters which play an important role in determining the $T_c$.

(4) Critical magnetic field($H_c$) and critical current density(Jc)

The lower- and upper-critical magnetic fields, $H_{c1}$ and $H_{c2}$ were measured at liquid helium temperature by a standard four-probe method using a superconducting solenoid for magnetic fields up to about $7.2 \times 10^6$ A/m(90 kOe) applied transversely to the specimen in a liquid helium bath. Typical resistance-magnetic field curves for the Nb-, Mo-, W- and Ti-Nb-based amorphous alloys with $T_c$ above 4.5 K are shown in Figs. 17 to 19. The $H_{c2}$(onset) value obtained is about $2.3 \times 10^6$ A/m for $Nb_{55}Mo_{25}Si_{20}$, $9.2 \times 10^5$ A/m for $Nb_{70}Mo_{10}Si_{20}$, $6.4 \times 10^5$ A/m for $Nb_{80}Si_{16}Ge_4$, $6.0 \times 10^6$ A/m for $Mo_{70}Si_{20}B_{10}$, $6.4 \times 10^5$ A/m for $W_{70}Si_{20}B_{10}$, $2.6 \times 10^6$ A/m for $Ti_{55}Nb_{30}Si_{15}$ and $3.1 \times 10^6$ A/m for $Ti_{45}Nb_{40}Si_{15}$, following a general tendency[35] that the higher the $T_c$, the higher is $H_{c2}$. In addition, one can notice in these figures that the $H_{c2}$ values are much higher compared with the $H_{c1}$ values.

From Ginzburg-Landau(GL) theory[36], $H_{c2}$ and $H_{c1}$ are expressed as

$$H_{c2} = \sqrt{2}\,\kappa\, H_c \qquad (1)$$

$$H_{c1} = (1/\sqrt{2}\,\kappa)(\log \kappa + 0.08)\, H_c, \qquad (2)$$

where $H_c$ is the critical magnetic field at 0 K and $\kappa$ is the Ginzburg-Landau parameter given by the following equation;

$$\kappa = \frac{\lambda(T)}{\xi(T)} = 0.725\frac{\lambda_L(0)}{\ell} \qquad (3)$$

$\lambda$ is the penetration length of magnetic field, $\xi$ the coherence length, $\lambda_L$ the penetration length of London, and $\ell$ the mean free path of electrons. It has been reported[37] that the value of $\kappa$ for amorphous superconductors is very large(50-100) because of a small value of the electron mean free path. As is evident from the equations (1) and (2), it is presumed that the Nb-, Mo-, W- and Ti-Nb-based amorphous alloys have a high $H_{c2}$ value and a low

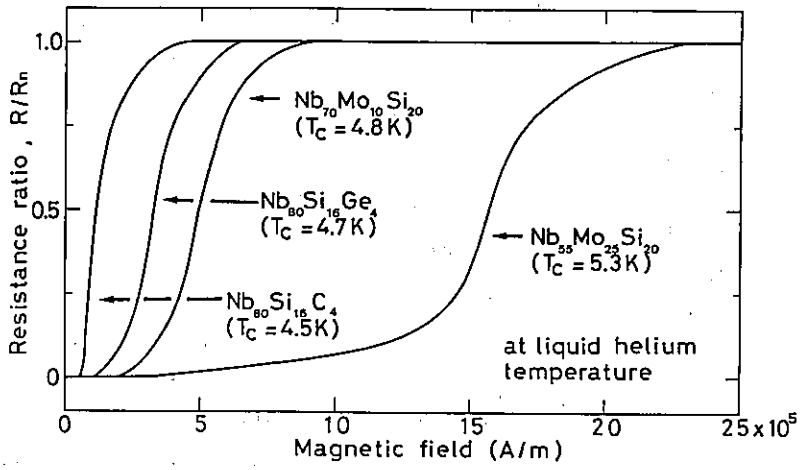


Fig. 17 Resistance ratio R/Rn as a function of magnetic field at liquid helium temperature for several Nb-based amorphous alloys.

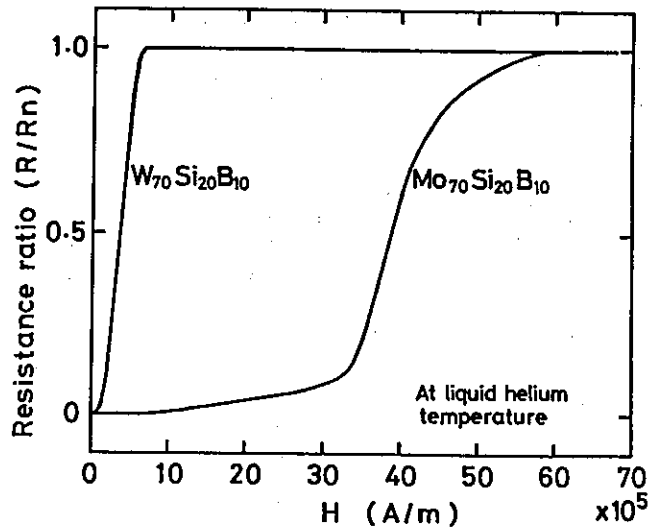


Fig. 18 Resistance ratio R/Rn as a function of magnetic field at liquid helium temperature for $Mo_{70}Si_{20}B_{10}$ and $W_{70}Si_{20}B_{10}$ amorphous alloys.

$H_{c1}$ value due to the large $\kappa$ value. These results indicate that the present amorphous alloys can be classified as type-II superconductors, similar to the melt-quenched other amorphous alloys.

In our investigations, no information has been obtained about the temperature dependence of $H_{c2}$ for the Nb-, Mo-, W- and Ti-Nb-based amorphous alloys. However, other papers[23,29] have shown that there exists a linear relationship between $H_{c2}$ and tempera-

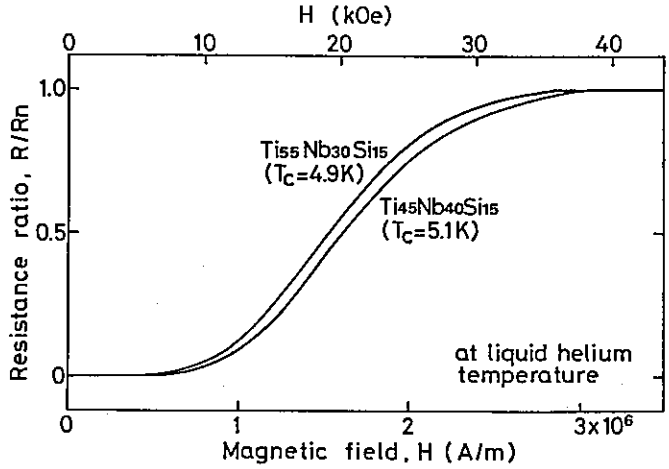


Fig. 19 Resistance ratio R/Rn as a function of magnetic field at liquid helium temperature for $Ti_{55}Nb_{30}Si_{15}$ and $Ti_{45}Nb_{40}Si_{15}$ amorphous alloys.

ture. Based on this fact, the value of $dH_{c2}/dT$ can be estimated for the amorphous alloys of Nb-Mo-Si, Nb-Si-B, Nb-Si-C, Nb-Si-Ge, Mo-Si-B, W-Si-B and Ti-Nb-Si. The results are shown in Table 2 together with other superconducting properties. The value of

Table 2 Superconducting transition temperature($T_c$), transition width($\Delta T_c$), critical current density($J_c$), upper critical magnetic field($H_{c2}$) and temperature dependence of $H_{c2}$ ($dH_{c2}/dT$) for several refractory metal-based amorphous alloys.

| Alloy system (at%) | $T_c$ (K) | $\Delta T_c$ (K) | $J_c$(A/cm$^2$) $\times 10^3$ | $H_{c2}$(A/m) $\times 10^5$ | $dH_{c2}/dT$(A·m$^{-1}$/K) $\times 10^5$ |
|---|---|---|---|---|---|
| $Nb_{70}Mo_{10}Si_{20}$ | 4.8 | 0.3 | - | 9.2 | 23 |
| $Nb_{60}Mo_{20}Si_{20}$ | 5.0 | 0.3 | 4.6 | - | - |
| $Nb_{55}Mo_{25}Si_{20}$ | 5.3 | 0.4 | 11 | 23 | 23 |
| $Nb_{80}Si_{16}B_4$ | 4.7 | 0.3 | - | - | - |
| $Nb_{80}Si_{16}C_4$ | 4.5 | 0.3 | - | 4.3 | 22 |
| $Nb_{80}Si_{16}Ge_4$ | 4.7 | 0.3 | - | 6.4 | 19 |
| $Mo_{70}Si_{20}B_{10}$ | 6.8 | 0.3 | 5 | 60 | 23 |
| $W_{70}Si_{20}B_{10}$ | 4.5 | 0.3 | 3 | 6.4 | 21 |
| $Ti_{55}Nb_{30}Si_{15}$ | 4.9 | 0.5 | 0.27 | 26 | 60 |
| $Ti_{45}Nb_{40}Si_{15}$ | 5.1 | 0.5 | 0.30 | 31 | 48 |

$dH_{c2}/dT$ is about $2.2 \times 10^6$ $A \cdot m^{-1}/K$ for the Nb-, Mo- and W-based alloys and about $5.4 \times 10^6$ $A \cdot m^{-1}/K$ for Ti-Nb-Si alloys. These values are much larger than those[6] for vapor-deposited amorphous transition pure metals and ordinary crystalline superconducting alloys such as Ti-Nb[24] and $Nb_3Sn$[1]. Such a large value of the amorphous alloys also seems to be due to the fact that the value of $\kappa$ is much larger compared with that of crystalline superconductors. Further, one can notice in Table 2 that the values of $dH_{c2}/dT$ for Ti-Nb-Si alloys are higher than the present data for $(Nb\text{-}Mo)_{80}Si_{20}$, $Nb_{80}(Si\text{-}M)_{20}$(M=B, C and Ge), $Mo_{70}Si_{20}B_{10}$ and $W_{70}Si_{20}B_{10}$ amorphous alloys and the previous data (about $2.1 \times 10^6$ $A \cdot m^{-1}/K$)[23] for $(Mo\text{-}Ru)_{80}P_{20}$ amorphous alloys. For an extended Ginzburg-Landau-Abrikosov-Gorkov(GLAG) theory[38,39], it is expressed that $dH_{c2}/dT$ is dependent on the residual resistivity($\rho$), the electron-phonon bare density of states N(0) at the Fermi level ($E_f$=0) and the electron-phonon coupling constant $\lambda$. Hence, for understanding the reason why the Ti-Nb-Si alloys possess the large values of $dH_{c2}/dT$, it is necessary to measure the values of $\rho$, N(0) and $\lambda$. Detailed investigations on this point are in progress at present.

The critical current density $J_c$ was measured for the amorphous alloys with $T_c$ above 4.7 K. The critical current was defined as the current at which a measurable voltage(1 $\mu$V) appeared across a 55 mm-length of the specimen in a liquid helium bath at no applied field. The critical current density $J_c$ was obtained by dividing the critical current with the cross-sectional area of the specimen. The $J_c$ value obtained is about $4.6 \times 10^3$ $A/cm^2$ for $Nb_{60}Mo_{20}Si_{20}$, about $1.1 \times 10^4$ $A/cm^2$ for $Nb_{55}Mo_{25}Si_{20}$, about $4.4 \times 10^3$ $A/cm^2$ for $Nb_{80}Si_{16}B_4$, $5 \times 10^3$ $A/cm^2$ for $Mo_{70}Si_{20}B_{10}$, $3 \times 10^3$ $A/cm^2$ for $W_{70}Si_{20}B_{10}$ and $3 \times 10^2$ $A/cm^2$ for $Ti_{45}Nb_{40}Si_{15}$. Further, $J_c$ was measured in external applied magnetic fields(H) in a liquid helium bath. As an example, Fig. 20 shows the critical current density $J_c(H)$ as a function of H for $Ti_{55}Nb_{30}Si_{15}$ amorphous alloy. For H=0, $J_c$ is found to be about 270 $A/cm^2$. For H>0, $J_c$ is observed to fall very rapidly with increasing H. For example, at $H \simeq 0.5\ H_{c2}$, $J_c$ is of the order of 150 $A/cm^2$. Such small values seem to result from the fact that the amorphous phase does not contain the pinning centers such as grain boundaries, dislocations, precipitates and other defects and is quite homogeneous on the scale of coherence length($\xi$=3-10 nm)[37].

However, $J_c(H)$ value improves by the introduction of a small volume fraction of crystalline precipitates into the amorphous superconducting matrix. Figure 21[40] shows $J_c(H)$ as a function of H at 4.2 K for amorphous $Ti_{55}Nb_{30}Si_4B_{11}$ and $Ti_{57}Nb_{30}Si_{10}B_3$ samples containing crystalline phases with bcc structure. The critical current decreases much more slowly with increasing magnetic field compared with that shown in Fig. 20. For H=0, $J_c$ is of order of $7 \times 10^4$ $A/cm^2$ for $Ti_{55}Nb_{30}Si_4B_{11}$ and $2 \times 10^4$ $A/cm^2$ for $Ti_{57}Nb_{30}Si_{10}B_3$, and also $H_{c2}$ is more than $6.4 \times 10^6$ A/m(80 kOe) for $Ti_{55}Nb_{30}Si_4B_{11}$. These results indicate that the introduction of crystalline phase into the amorphous matrix results in a remarkable increase of flux pinning forces.

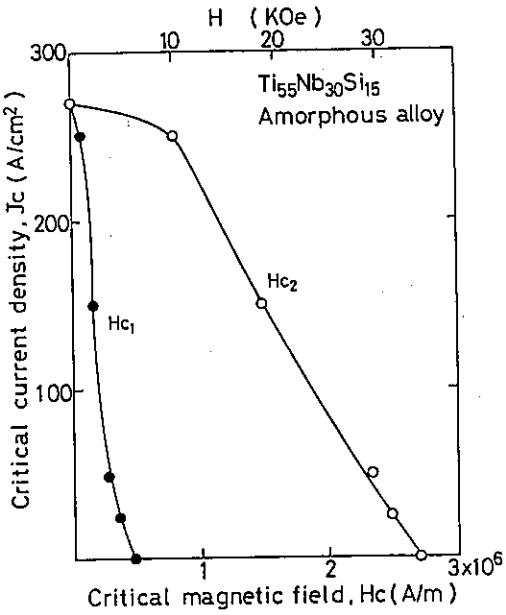


Fig. 20 Critical current density($J_c$) of $Ti_{55}Nb_{30}Si_{15}$ amorphous alloy as a function of magnetic field applied normal to the direction of current flow.

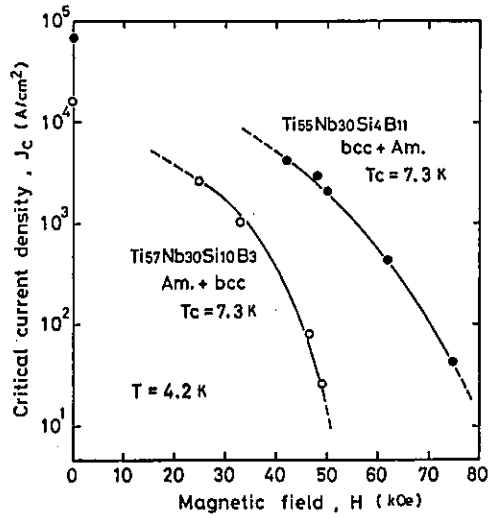


Fig. 21 Critical current density($J_c$) of $Ti_{55}Nb_{30}Si_4B_{11}$ and $Ti_{57}Nb_{30}Si_{10}B_3$ amorphous alloys as a function of magnetic field applied normal to the direction of current flow.

## 6. SUPERCONDUCTING PROPERTIES OF THE ALLOYS CRYSTALLIZED FROM THE AMORPHOUS STATE

By crystallization from the amorphous state it is possible to produce a metastable phase unobtainable by standard metallurgical techniques. In addition, with a proper choice of heat treatments it is possible to obtain a very fine grain structure. Especially, it is expected that the A-15 type $Nb_3Si$[1] or $V_3Si$[1] compound with a high $T_c$ and $H_{c2}$ precipitates in the Nb-Si, Ti-Nb-Si and Ti-V-Si alloys crystallized from the amorphous state. The aim of this section is to present details of the crystallization behavior of their amorphous phases and the relation between the microstructure and the superconducting properties of these alloys.

### (1) $Nb_{80}Si_{20}$ binary alloy

#### (a) Crystallization behavior

The structural change of the alloy upon annealing is shown in Fig. 22. As seen in the figure, after annealing at 873 K for 10 h an oval-shaped crystal appears in the amorphous matrix. With further heating the crystal grows rapidly in the remaining amorphous phase and then complete devitrification occurs at about 973 K, as shown in Fig. 22 (a)-(c). Above about 973 K, this crystal decomposes into two stable phases of bct $Nb_3Si$ and bcc Nb, as shown in Fig. 22 (d). The detailed analysis of oval-shaped metastable crystal was made due to the possibility that the compound $Nb_3Si$, if it was formed in the cubic A-15 structure, would have a superconducting transition temperature($T_c$) in excess of 25 K[1]. One example of the results is shown in Fig. 23. The crystals with 0.3-0.5 μm in diameter containing a large amount of internal defects are seen in Fig. 23 (a). The selected area diffraction patterns (b) and (c) taken from the crystals in Fig. 23 (a) show clearly that the crystal has a body-centered tetragonal structure with a=1.017 nm and c=0.516 nm which corresponds to equilibrium bct $Nb_3Si$ compound with a=1.021 nm and c=0.519 nm[41]. Within the present investigations, the compound $Nb_3Si$ with the cubic A-15 structure could not be seen in both as-quenched and annealed states.

#### (b) Transition temperature($T_c$)

Figure 24 shows the change in the $T_c$ of $Nb_{80}Si_{20}$ amorphous alloy upon heating together with the crystal structure identified by X-ray diffraction. An open circle represents the amorphous single phase, semiopen circle the coexistence of bct $Nb_3Si$ compound and amorphous phase, and filled circle the equilibrium phases-bct $Nb_3Si$ and bcc Nb. The value in bracket represents the $T_c$. As seen in the figure, in the aged amorphous state and in the mixed state of amorphous and $Nb_3Si$ compound the values of $T_c$ are

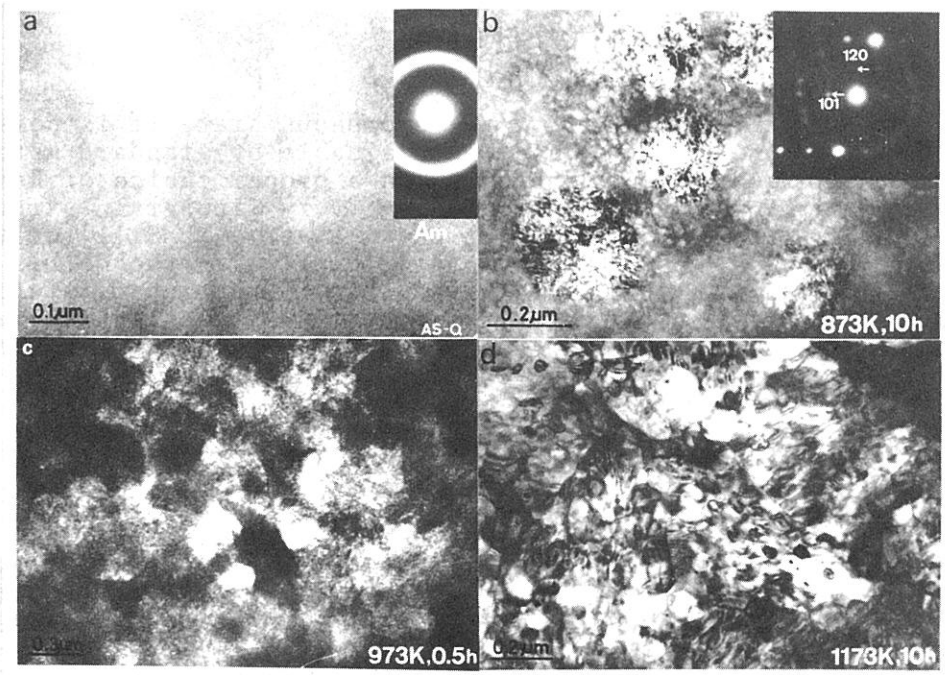


Fig. 22 Transmission electron micrographs and selected area diffraction patterns showing the microstructures of $Nb_{80}Si_{20}$ amorphous alloy heated for different periods at various temperatures.

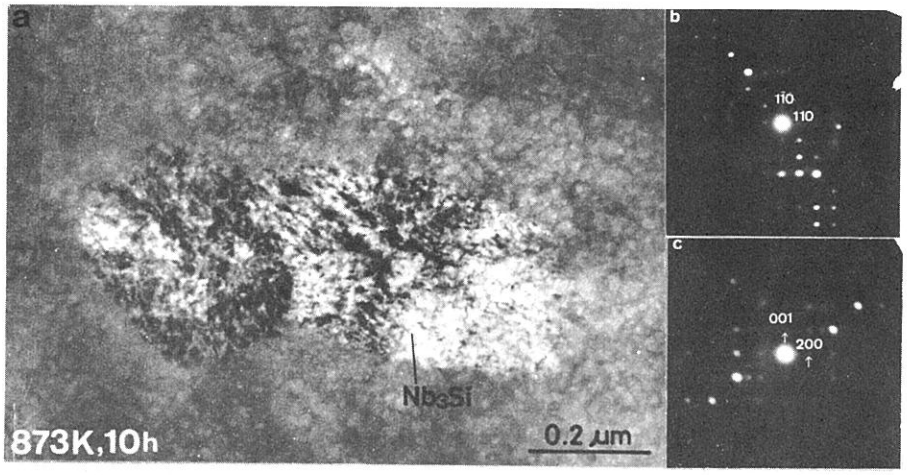


Fig. 23 The morphology and crystalline structures of $Nb_3Si$ compound for $Nb_{80}Si_{20}$ amorphous alloy heated for 10 h at 873 K. (a) bright field image, (b) and (c) selected area diffraction patterns taken from the crystals in the photograph (a). The normals to the crystals are [001] and [010], respectively.

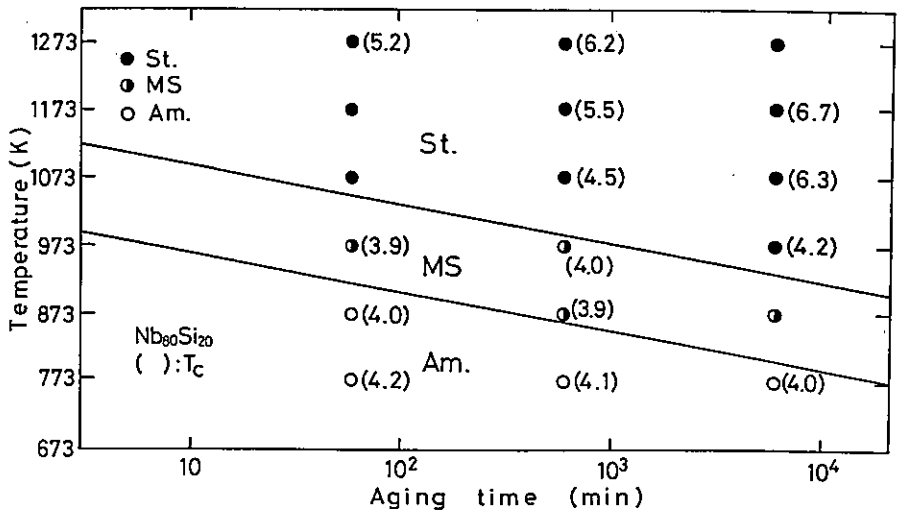


Fig. 24 The superconducting transition temperature($T_c$) of $Nb_{80}Si_{20}$ amorphous alloy annealed for different periods at various temperatures.

in the range of 3.9-4.2 K and are slightly lower compared with that of the as-quenched amorphous phase. The transformation to the equilibrium phases results in an increase in $T_c$ from 4.0 K to about 6.7 K. Thus, the $T_c$ in the crystalline state is fairly high compared with that in the amorphous state with the same alloy composition. The increase in $T_c$ after crystallization is attributed to the precipitation of a bcc Nb-phase because the bct $Nb_3Si$ compound is nonsuperconducting above 4.2 K.

Hasegawa and Tanner[42] have reported that partially crystallized amorphous $Zr_{65}Nb_{15}Be_{20}$ alloy obtained by liquid quenching exhibits a $T_c$ value of 6.85 K. This high $T_c$ value has been attributed to a proximity effect arising from a dispersion of crystalline Zr-rich Zr(Nb) bcc particles having 100-300 nm diameter and average spacings of 200 nm or less embedded in a amorphous Be-Zr-Nb matrix. This result implies that in the $Nb_3Si$-plus-amorphous state the Nb-Si alloys would be a superconductor with a high-transition temperature, if $Nb_3Si$ had a A-15 structure and dispersed in an appropriate particle size and spacing state in the amorphous matrix.

(2) Ti-Nb-Si and Ti-V-Si ternary alloys

(a) Crystallization behavior

The general features of the DTA curves for Ti-Nb-Si and Ti-V-Si alloys are exemplified in Figs. 25 and 26, wherein two exothermic peaks are seen, indicating that there exist two stages of crystallization for both the alloy systems. Figures 27 and 28

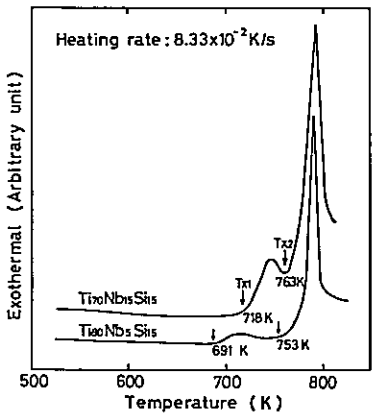


Fig. 25 Differential thermal analysis curves of $Ti_{80}Nb_5Si_{15}$ and $Ti_{70}Nb_{15}Si_{15}$ amorphous alloys.

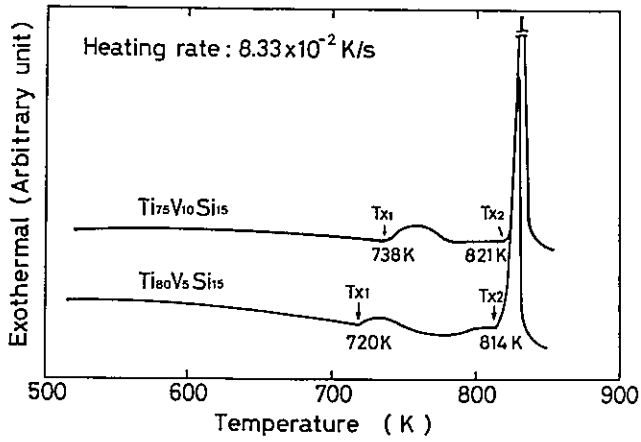


Fig. 26 Differential thermal analysis curves of $Ti_{80}V_5Si_{15}$ and $Ti_{75}V_{10}Si_{15}$ amorphous alloys.

show transmission electron micrographs of $Ti_{70}Nb_{15}Si_{15}$ and $Ti_{80}V_5Si_{15}$ alloys annealed for different periods at specified temperatures, which correspond to the beginning temperatures of the first and the second exothermic peaks on the DTA curve. Featureless structure and several haloes, which are typical feature of the amorphous material, are seen in the figures (a) and (b). There is not any observable change in the amorphous structure up to about 710 K for $Ti_{70}Nb_{15}Si_{15}$ and about 720 K for $Ti_{80}V_5Si_{15}$. In each specimen annealed for 10 min at 763 and 723 K, fine globular or elliptical precipitates are seen over the entire area of their specimens, as seen in the figures(c). The growth rate of these crystals is extremely slow and their average size is less than about 15 nm. In the diffraction patterns(d), some reflection spots from these crystals are superimposed in the rings from amorphous phase. Both the crystalline phases have a bcc structure which corresponds to a β-Ti(Nb) or β-Ti(V) solid solution. The lattice parameter is a=0.328 nm for $Ti_{70}Nb_{15}Si_{15}$ and a=0.326 nm for $Ti_{80}V_5Si_{15}$. Since any phase with a bcc structure does not exist in Ti-Nb and Ti-V equilibrium phase diagrams at room temperature, these phases can be considered a metastable phase(MS-I) representing the enhanced solid solubility of Nb or V in each β-Ti. The extremely slow growth of the MS-I phase is supposed to be probably due to an enrichment of silicon content in the amorphous phase. In both the specimens annealed for 60 min at 763 K for $Ti_{70}Nb_{15}Si_{15}$ and at 813 K for $Ti_{80}V_5Si_{15}$ oval-shaped crystals (MS-II phase) are seen over the entire area of the figures(e), in addition to the MS-I phase. From the electron diffraction patterns (f), the MS-II phase is $Nb_3Si$ having a bct structure with a=1.021 nm and c=0.519 nm for $Ti_{70}Nb_{15}Si_{15}$ and $Ti_5Si_3$ having a hexagonal structure with a=0.747 nm and c=0.516 nm for $Ti_{80}V_5Si_{15}$.

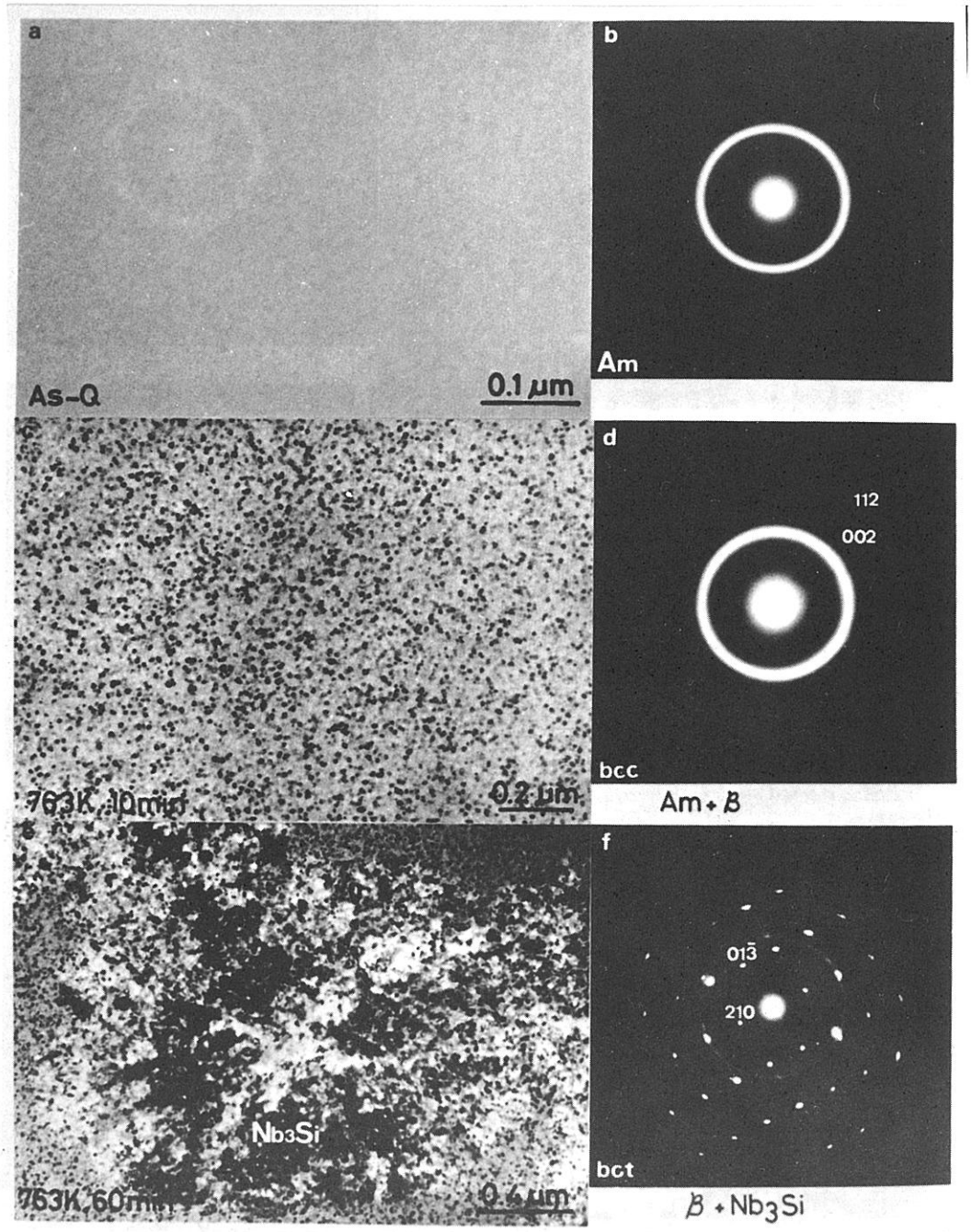


Fig. 27 Transmission electron micrographs and selected area diffraction patterns showing the as-quenched(a and b) and annealed(c, d, e and f) structure of $Ti_{70}Nb_{15}Si_{15}$ amorphous alloy.

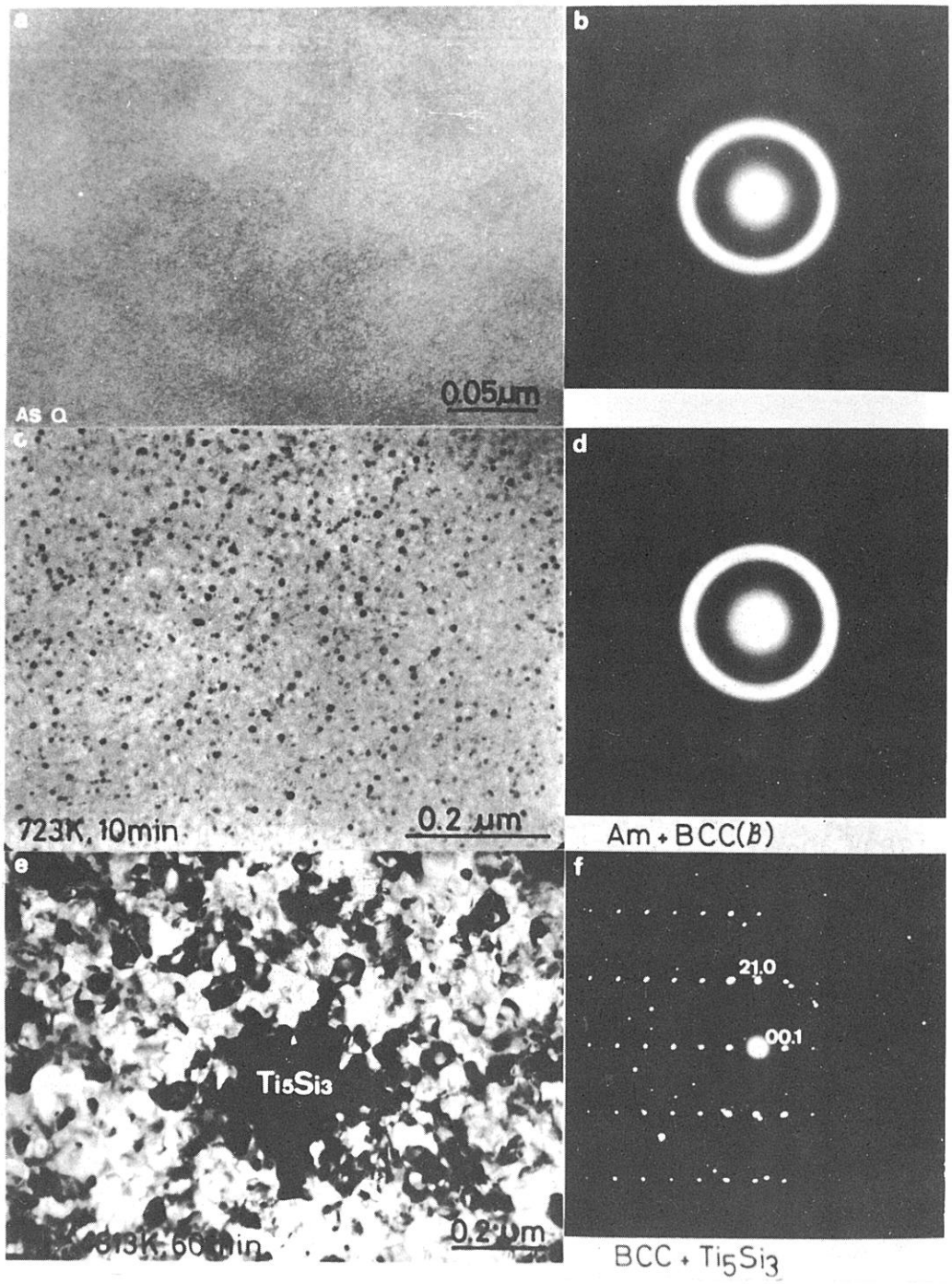


Fig. 28 Transmission electron micrographs and selected area diffraction patterns showing the as-quenched(a and b) and annealed(c, d, e and f) structures of $Ti_{80}V_5Si_{15}$ amorphous alloy.

At higher annealing temperatures, their MS-I phases transform to the hcp α-Ti stable phase. As an example, microstructure consisting of α-Ti and $Nb_3Si$ in $Ti_{70}Nb_{15}Si_{15}$ alloy annealed for 1 h at 833 K is shown in Fig. 29, wherein the α-Ti phase contains a large number of fine planar faults. Additionally, the hexagonal omega (ω) phase with a=0.295 nm and c=0.467 nm was sometimes observed in the temperature range of 700 to 900 K, which corresponds to the transformation range from the bcc β-phase to the hcp α-phase. However, we could not obtain detailed information about the transformation process among β, α and ω phases. Within this investigation, the compound $Nb_3Si$ or $V_3Si$ with the cubic A-15 structure could not be seen in the annealed samples. The above observations indicate that a broad, low intensity peak at the low temperature side in the DTA curves corresponds to the precipitation of the bcc β-phase(MS-I) from the amorphous phase and a narrow, high intensity peak at the higher temperature side is due to the transition of the remaining amorphous phase to the MS-II phase, i.e., bct-$Nb_3Si$ for Ti-Nb-Si alloy and hexagonal $Ti_5Si_3$ compound for Ti-V-Si alloy. Such a crystallization process, i.e., Am. ⟶ Am. + MS-I ⟶ MS-I + MS-II ⟶ Stable, agrees well with those of metal-metalloid system [4,43] as well as metal-metal system of Co-Ti [44].

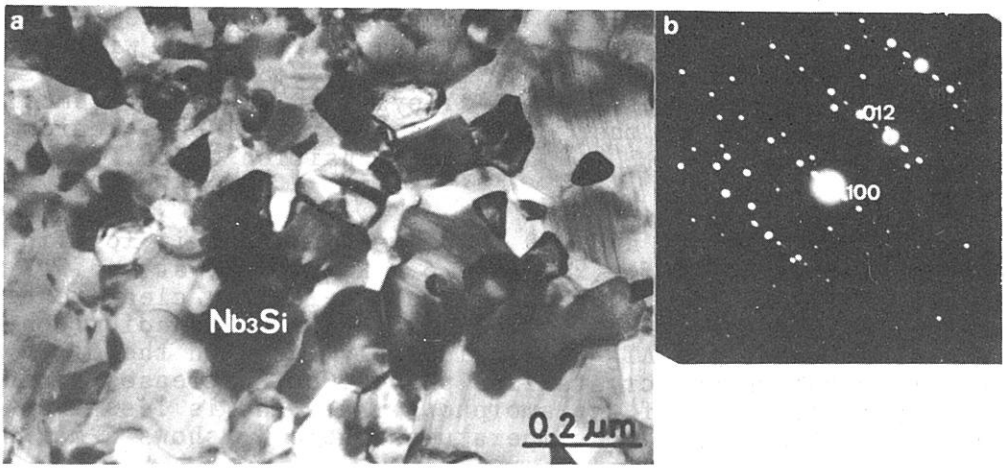


Fig. 29 Transmission electron micrograph and selected area diffraction pattern of $Ti_{70}Nb_{15}Si_{15}$ amorphous alloy annealed for 1 h at 833 K.

(b) Transition temperature($T_c$)

The $T_c$ and $\Delta T_c$ of Ti-Nb-Si and Ti-V-Si alloys annealed for 1 h at various temperatures are plotted in Figs. 30 and 31 as a function of annealing temperature. As seen in these figures, $T_c$ increases rapidly with increasing annealing temperature after crystallization, reaches a maximum value at appropriate temperatures and with continued annealing decreases. The maximum $T_c$ for $Ti_{85-x}Nb_xSi_{15}$ system is about 4.8 K for x=5 at%, 7.3 K for x=15

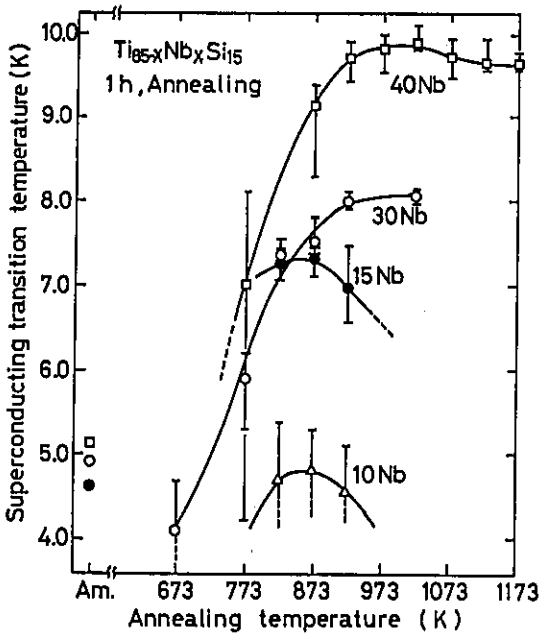


Fig. 30 Changes in superconducting transition temperature ($T_c$) and transition width ($\Delta T_c$) for $Ti_{85-x}Nb_xSi_{15}$ amorphous alloys with annealing temperature. Vertical bars represent the transition width.

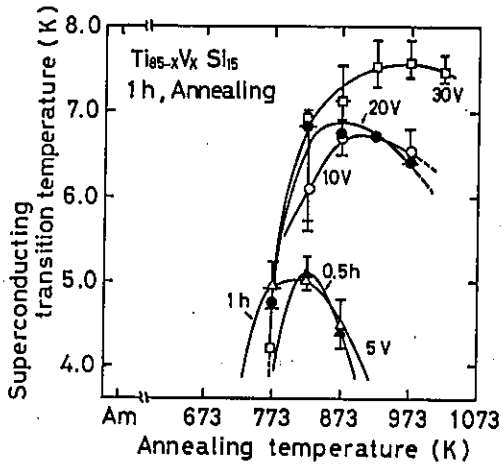


Fig. 31 Changes in superconducting transition temperature ($T_c$) and transition width ($\Delta T_c$) for $Ti_{85-x}V_xSi_{15}$ amorphous alloys with annealing temperature. Vertical bars represent the transition width.

at%, 8.1 K for x=30 at% and 9.9 K for x=40 at% and it for $Ti_{85-x}V_xSi_{15}$ system is 5.1 K for x=5 at%, 6.7 K for x=10 at%, 6.9 K for x=20 at% and 7.6 K for x=30 at%. Thus, there is a clear tendency that the $T_c$ increases with increasing niobium or vanadium content. On the other hand, the $\Delta T_c$ is considerably large in the mixed state of amorphous and crystalline phases, but decreases rapidly after crystallization of the amorphous phase and is less than about 0.5 K at appropriate temperatures where $T_c$ shows a maximum value.

The above-described transmission electron microscopic observations indicate that the crystalline superconductors consist of bcc β-Ti(Nb) and bct $Nb_3Si$ for the Ti-Nb-Si alloys and bcc β-Ti(V) and hexagonal $Ti_5Si_3$ for the Ti-V-Si alloys. Since the bct $Nb_3Si$[41] and hexagonal $Ti_5Si_3$ [45] phases are nonsuperconducting above 4.2 K, it is concluded that the high $T_c$ values of the crystalline Ti-Nb-Si and Ti-V-Si alloys are attributed to the β-Ti(Nb) and β-Ti(V) solid solution, respectively, similar to the mechanism for the conventional superconducting Ti-Nb[25] and Ti-V[46] binary alloys. It has been shown[24,25] that $T_c$ and $H_c$ depend largely on the Nb or V content in the β phase. According to their results,

$T_c$ of crystalline Ti-Nb binary alloys is less than 4.2 K for $Ti_{90}Nb_{10}$ and $Ti_{85}Nb_{15}$ and is about 6.8 K for $Ti_{70}Nb_{30}$ and about 8.0 K for $Ti_{60}Nb_{40}$ and it of Ti-V alloys is less than 4.2 K for $Ti_{80}V_{20}$ and is about 6.2 K for $Ti_{70}V_{30}$. The $T_c$ values of Ti-Nb-Si and Ti-V-Si alloys are much higher compared with those for Ti-Nb and Ti-V binary alloys with the same niobium or vanadium concentration. This difference is remarkable especially for the alloys with low niobium or vanadium concentrations such as $Ti_{70\text{-}75}Nb_{10\text{-}15}Si_{15}$ and $Ti_{75\text{-}80}V_{5\text{-}10}Si_{15}$. The reason for this difference can be attributed to the appearance of the metastable β-Ti(Nb) or β-Ti(V) solid solution which can not be found in the equilibrium phase diagram of Ti-Nb or Ti-V binary alloys[47] at room temperature. This hypothesis receives support from the fact that the $T_c$ values of their alloys fall rapidly by the transformation of bcc β-phase to hcp α-stable phase. It is also noticed that $T_c$ decreases after reaching the peak value more drastically at lower niobium or vanadium contents. This may be due to the decreasing volume fraction of the α-phase at higher niobium or vanadium content. Further, we estimated the niobium or vanadium concentration in the β-phase from the $T_c$ values based on the previous data[22,23]. The much higher $T_c$ values compared with those of Ti-Nb or Ti-V binary alloys with the same niobium or vanadium content seem to be attributable to the fact that the metastable β solid solutions contain niobium or vanadium much in excess of the equilibrium limit.

The maximum $T_c$ values of Nb-Si, Ti-Nb-Si and Ti-V-Si crystal-

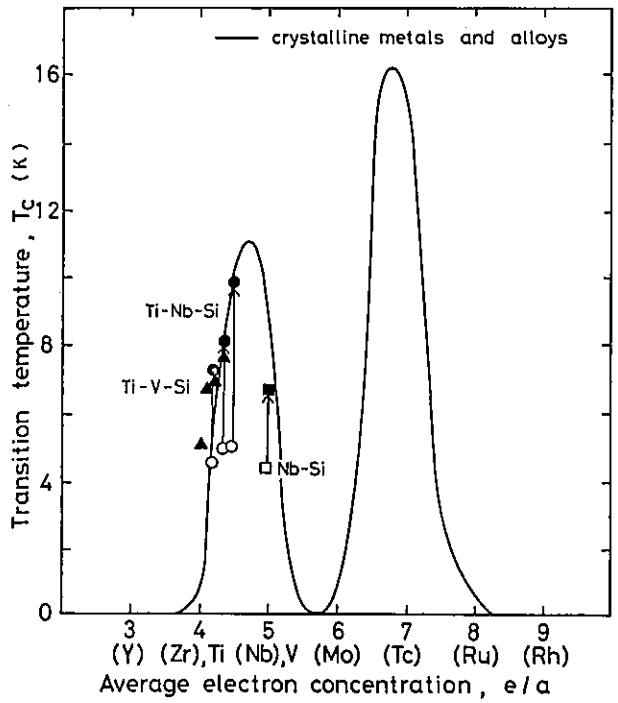


Fig. 32 Superconducting transition temperature($T_c$) vs. electron per atom ratio(e/a) for the 4d transition-metal series.

line alloys are plotted as a function of the average outer electron concentration[e/a] of the transition metal components in Fig. 32, wherein the values of $T_c$ for amorphous Nb-Si and Ti-Nb-Si alloys are also included. Further, these data are compared with the variation of $T_c$ for crystalline transition metals and alloys which is well known as Matthias rule. From this figure, it is seen that the $T_c$ of the amorphous alloys increases remarkably upon crystallization and their values agree well with those expected by the Matthias rule.

(c) Critical magnetic field($H_c$) and critical current density($J_c$)

The critical current density $J_c$ was measured at external applied magnetic field(H) in a liquid helium bath. Figures 33 to 37 show the critical current density $J_c(H)$ as a function of H for $Ti_{70}Nb_{15}Si_{15}$, $Ti_{55}Nb_{30}Si_{15}$, $Ti_{50}Nb_{35}Si_{15}$, $Ti_{65}V_{20}Si_{15}$ and $Ti_{55}V_{30}Si_{15}$ amorphous alloys annealed for different periods at various temperatures. As seen in these figures, Ti-Nb-Si alloys possess much higher $J_c(H)$ values compared with Ti-V-Si alloys. For example, for $H=5.6 \times 10^6$ A/m(70 kOe), the $J_c$ is about $5 \times 10^3$ A/cm$^2$ for $Ti_{70}Nb_{15}Si_{15}$, about $1 \times 10^4$ A/cm$^2$ for $Ti_{55}Nb_{30}Si_{15}$ and about $4.7 \times 10^4$ A/cm$^2$ for $Ti_{50}Nb_{35}Si_{15}$ and about $2 \times 10^3$ A/cm$^2$ for $Ti_{55}V_{30}Si_{15}$. Also, one can notice the tendency that $J_c(H)$ values

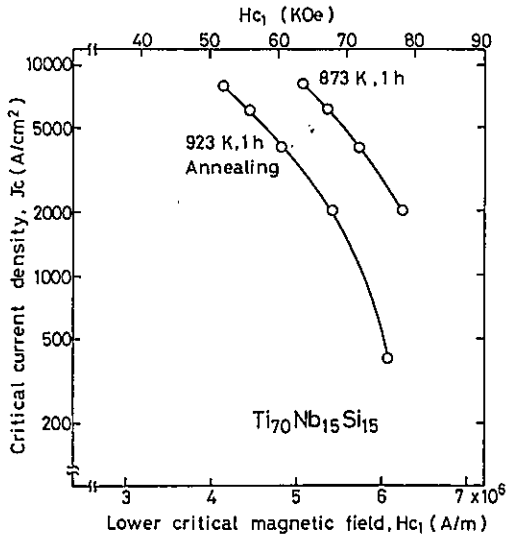


Fig. 33 Critical current density($J_c$) of $Ti_{70}Nb_{15}Si_{15}$ amorphous alloy annealed for 1 h at 873 and 923 K as a function of magnetic field applied normal to the direction of current flow.

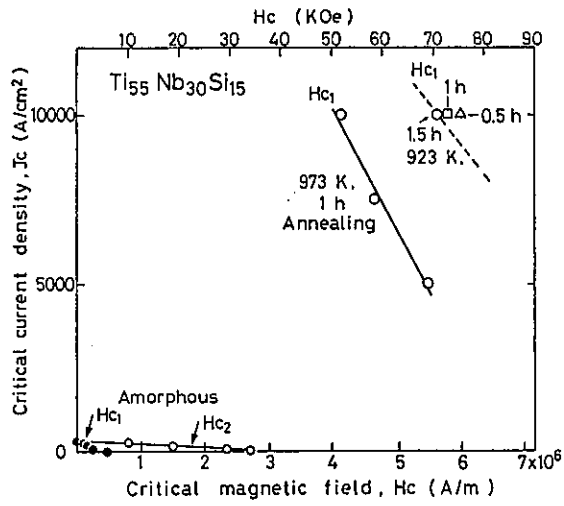


Fig. 34 Critical current density($J_c$) of $Ti_{55}Nb_{30}Si_{15}$ amorphous alloy annealed for 0.5 and 1 h at 923 and 973 K as a function of magnetic field applied normal to the direction of current flow.

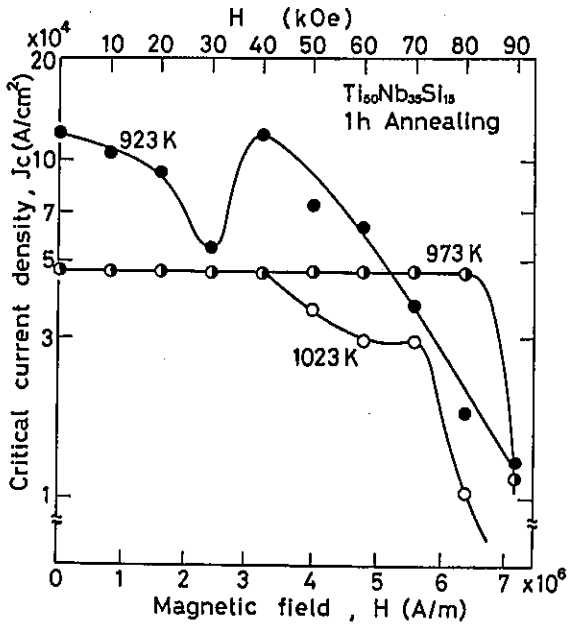


Fig. 35 Critical current density($J_c$) of $Ti_{50}Nb_{35}Si_{15}$ amorphous alloy annealed for 1 h at various temperatures as a function of magnetic field applied normal to the direction of current flow.

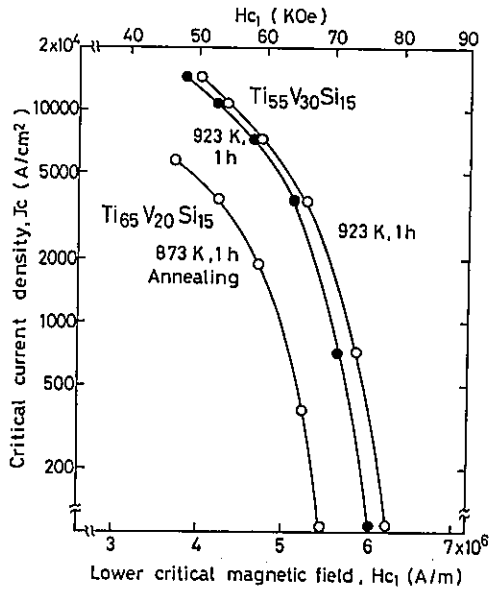


Fig. 36 Critical current density($J_c$) of $Ti_{65}V_{20}Si_{15}$ and $Ti_{55}V_{30}Si_{15}$ amorphous alloys annealed for 1 h at 873 and 923 K as a function of magnetic field applied normal to the direction of current flow.

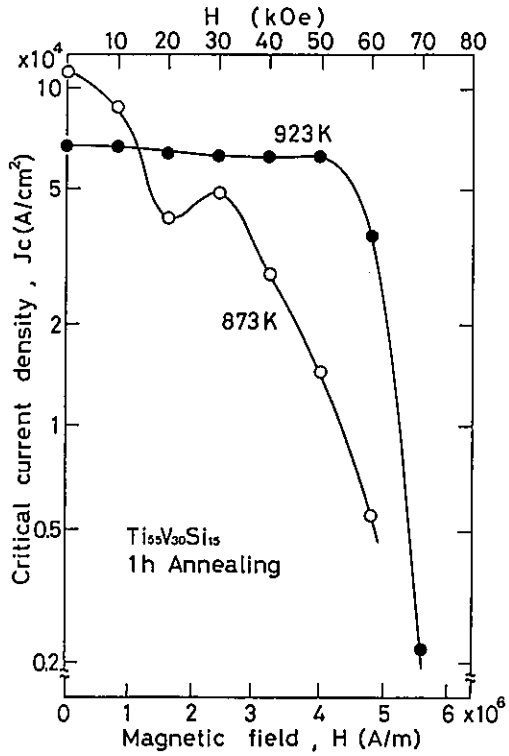


Fig. 37 Critical current density($J_c$) of $Ti_{55}V_{30}Si_{15}$ amorphous alloy annealed for 1 h at 873 and 923 K as a function of magnetic field applied normal to the direction of current flow.

increase with increasing niobium or vanadium content. In addition, as seen in Fig. 35, the pinning force which is given by the area under $J_c$-H curve shows a maximum value at an appropriate temperature (about 973 K for $Ti_{50}Nb_{35}Si_{15}$ alloy). The underaging at 923 K results in high $J_c$ of about $1 \times 10^5$ A/cm$^2$ for H less than about $3.2 \times 10^6$ A/m(40 kOe) and the overaging at 1023 K results in $J_c$ values less than $5 \times 10^4$ A/cm$^2$ over all the H range. In general, it is well known that $J_c$(H) is closely related to the microstructure of the alloy. Figure 38 shows the structure of $Ti_{50}Nb_{35}Si_{15}$ amorphous alloys annealed for 1 h at 923, 973 and 1023 K. All structures consist of bcc β-Ti(Nb) and bct $Nb_3Si$ phase and the average particle diameter of the $Nb_3Si$ phase is about 50 nm at 923 K, 90 nm at 973 K and 200 nm at 1023 K. These structures indicate that the high $J_c$(H) value for $Ti_{50}Nb_{35}Si_{15}$ alloy annealed for 1 h at 973 K is attributed to a dispersion effect of the $Nb_3Si$ particles, having about 90 nm diameter and an average spacing of 100 nm or less, in bcc β-Ti(Nb) phase.

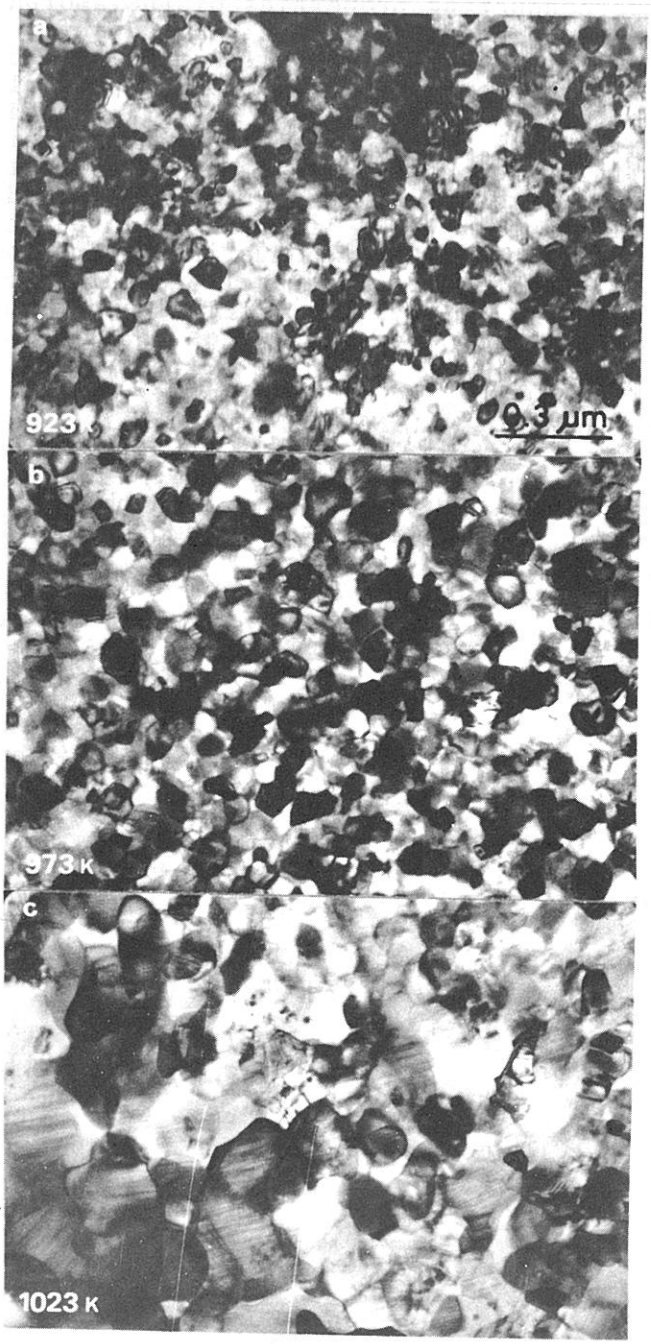


Fig. 38 Transmission electron micrographs of $Ti_{50}Nb_{35}Si_{15}$ amorphous alloy annealed for 1 h at 923 K(a), 973 K(b) and 1023 K(c).

## 7. CONCLUSION

The superconducting properties of the amorphous alloys characterized in the present paper are still insufficient for practical use. However, there is no well-established theoretical reason why the $T_c$ of amorphous superconductors should always be lower than those of crystalline alloys. We believe that it would be possible to find new amorphous alloys with transition temperatures higher than those reported in this review as well as good ductility through more extensive investigations. In addition, from the technological point of view, it is to be noted that melt quenching makes the processing of superconducting materials much simpler. Especially, the existence of a readily obtainable amorphous phase in the Ti-Nb-Si system seems to offer alternative means of fabricating superconducting tapes and wires.

## ACKNOWLEDGEMENTS

For the preparation of this review, the authors rely mainly upon results obtained by the authors and their coworkers, i.e., Messrs. S. Sakai, H. M. Kimura and A. Hoshi and Dr. Suryanarayana. The authors would like to express their grateful acknowledgement to them.

## REFERENCES


1) D. Dew-Hughes: Cryogenics, 15(1975), 435.
2) R. H. Willens, E. Buehler and B. T. Matthias: Phys. Rev., 159(1967), 327.
3) B. T. Matthias, V. B. Compton and E. Corenzwit: J. Phys. Chem. Solids, 19(1961), 130.
4) T. Masumoto and R. Maddin: Acta Met., 19(1971), 725.
5) W. Buckel and R. Hilsch: Z. Phys., 138(1954), 109.
6) G. Bergmann: Phys. Reports, 27C(1976), 161.
7) W. L. Johnson, S. J. Poon and P. Duwez: Phys. Rev. B, 11(1975) 150.
8) S. Sakai, H. M. Kimura, A. Inoue and T. Masumoto: Papers represented at the Meetings of the Japan Institute of Metals, October 1978, p. 236; April 1979, p. 190.
9) T. Masumoto, A. Inoue, S. Sakai, H. M. Kimura and A. Hoshi: Trans. JIM, 21(1980), 115.
10) A. Inoue, H. M. Kimura, T. Masumoto, C. Suryanarayana and A. Hoshi: J. Appl. Phys., to be published.
11) A. Inoue, C. Suryanarayana, T. Masumoto and A. Hoshi: Sci. Rep. Res. Inst. Tohoku University, A28(1980), No. 2, in press.
12) A. Inoue, H. M. Kimura, C. Suryanarayana, T. Masumoto and A. Hoshi: J. Mater. Sci., to be published.
13) A. Inoue, S. Sakai, H. M. Kimura, T. Masumoto and A. Hoshi: Scripta Met., 14(1980), No. 2, in press.
14) S. Sakai, A. Inoue, H. M. Kimura and T. Masumoto: Scripta Met., 14(1980), No. 3, in press.
15) A. Inoue, T. Masumoto, C. Suryanarayana and A. Hoshi: to be presented at the 4th Intern. Conf. on Liquid and Amorphous Metals, Grenoble, France, July 1980.
16) D. Turnbull: J. Phys. (Paris) Colloq., 35(1974), 1.
17) C. J. Smithells: Metals Reference Book, 5th Edition, p. 725, 780, 782, Butterworths, (1976).
18) A. Inoue, T. Masumoto and H. M. Kimura: J. Japan Inst. Metals, 42(1978), 303; Sci. Rep. Res. Inst. Tohoku University, A27 (1979), 159.
19) W. D. Forgeng and W. D. Forgeng, Jr.: Metals Handbook eighth edition, Metallography, Structures and Phase Diagram, p. 283, 334, ASM, (1973).
20) For example, T. Masumoto: Sci. Rep. Res. Inst. Tohoku University, A26(1977), 246.
21) C. C. Tsuei, W. L. Johnson, R. L. Laibowitz and J. M. Viggiano: Solid State Commun., 24(1977), 615.
22) M. M. Collver and R. H. Hammond: Phys. Rev. Lett., 30(1973), 92.
23) W. L. Johnson, S. J. Poon, J. Durand and P. Duwez: Phys. Rev. B, 18(1978), 206.
24) T. G. Berlincourt and R. R. Hake: Phys. Rev., 131(1963), 140.
25) J. V. Vetrano and R. W. Boom: J. Appl. Phys., 36(1965), 1179.
26) For example, W. L. Johnson: J. Appl. Phys., 50(1979), 1557.
27) For example, W. DeSorbo: Phys. Rev., 130(1963), 2177.
28) K. Togano and K. Tachikawa: Phys. Lett., 54A(1975), 205.
29) E. R. Domb and W. L. Johnson: J. Low Temp. Phys., 33(1978), 29.

30) H. Fujimori, T. Masumoto, Y. Obi and M. Kikuchi: Japan. J. Appl. Phys., 13(1974), 1889.
31) T. Egami, P. J. Flanders and C. D. Graham, Jr.: Appl. Phys. Letters, 26(1975), 128.
32) H. S. Chen, C. D. Ferris, E. M. Gyorgy, H. J. Leamy and R. C. Sherwood: Appl. Phys. Letters, 26(1975), 405.
33) T. Egami and P. J. Flanders: A.I.P. Conf. Proc., 29(1976), 220.
34) A. J. Drehman and W. L. Johnson: Phys. Stat. Sol., (a)52(1979), 499.
35) K. Maki and T. Tsuzuki: Phys. Rev. 139(1965), 868.
36) N. R. Werthamer, E. Helfand and P. C. Hohenberg: Phys. Rev., 147(1966), 295.
37) W. L. Johnson: Rapidly Quenched Metals III, Ed. B. Cantor, Vol. 2, The Metals Society, London (1978), p. 1.
38) G. Eilenberger and V. Ambegaokar: Phys. Rev., 168(1967), 332.
39) D. Rainer, G. Bergmann and V. Eckhardt: Phys. Rev. B, 8(1973), 5324.
40) A. Inoue, A. Hoshi, C. Suryanarayana and T. Masumoto: Scripta Met., to be published.
41) D. K. Deardorff, R. E. Siemens, P. A. Romans and R. A. McCune: J. Less-Common Metals, 18(1969), 11.
42) R. Hasegawa and L. E. Tanner: J. Appl. Phys., 49(1978), 1196.
43) For example, T. Masumoto, H. M. Kimura, A. Inoue and Y. Waseda: Mater. Sci. Eng., 23(1976).
44) A. Inoue, K. Kobayashi, C. Suryanarayana and T. Masumoto: Scripta Met., 14(1980), No. 1, in press.
45) A. Inoue, C. Suryanarayana and T. Masumoto: unpublished research.
46) C. H. Chang, K. P. Gupta, E. C. Van Reuth and P. A. Beck: Phys. Rev., 126(1962), 2030.
47) C. J. Smithells: Metals Reference Book, 5th Edition, p. 726, 793, Butterworths, (1976).